Article

Heat and carbon coupling reveals ocean warming due to circulation changes

Ben Bronselaer[1,2,3,4 ✉] & Laure Zanna[1,5]

Anthropogenic global surface warming is proportional to cumulative carbon emissions[1–3]; this relationship is partly determined by the uptake and storage of heat and carbon by the ocean[4]. The rates and patterns of ocean heat and carbon storage are influenced by ocean transport, such as mixing and large-scale circulation[5–10]. However, existing climate models do not accurately capture the observed patterns of ocean warming, with a large spread in their projections of ocean circulation and ocean heat uptake[8,11]. Additionally, assessing the influence of ocean circulation changes (specifically, the redistribution of heat by resolved advection) on patterns of observed and simulated ocean warming remains a challenge. Here we establish a linear relationship between the heat and carbon uptake of the ocean in response to anthropogenic emissions. This relationship is determined mainly by intrinsic parameters of the Earth system—namely, the ocean carbon buffer capacity, the radiative forcing of carbon dioxide and the carbon inventory of the ocean. We use this relationship to reveal the effect of changes in ocean circulation from carbon dioxide forcing on patterns of ocean warming in both observations and global Earth system models from the Fifth Coupled Model Intercomparison Project (CMIP5). We show that historical patterns of ocean warming are shaped by ocean heat redistribution, which CMIP5 models simulate poorly. However, we find that projected patterns of heat storage are primarily dictated by the pre-industrial ocean circulation (and small changes in unresolved ocean processes)—that is, by the patterns of added heat owing to ocean uptake of excess atmospheric heat rather than ocean warming by circulation changes. Climate models show more skill in simulating ocean heat storage by the pre-industrial circulation compared to heat redistribution, indicating that warming patterns of the ocean may become more predictable as the climate warms.

The increase in emissions of anthropogenic greenhouse gases such as CO_2 has led to rising atmospheric temperatures since pre-industrial times. The ocean absorbs most of the excess heat and some of the excess carbon, mitigating atmospheric warming[12]. However, the storage of heat and carbon by the ocean leads to adverse regional effects such as sea-level rise, coral bleaching and ocean acidification[8,10,13–16]. Ocean transport affects both global and regional ocean temperature and also carbon changes[9,17]. In particular, changes in ocean transport can shape ocean warming patterns[5,7,8,10]. Yet, directly assessing the effects of changing ocean currents on ocean warming both in observations and also in climate models[8] remains challenging. In addition, there is a lack of agreement between modelled and observed heat storage and also a large spread among different models in the simulated patterns of ocean heat storage—the causes for these discrepancies are difficult to attribute[11]. To diagnose the effect of changes in large-scale ocean circulation (namely, resolved advection) on ocean warming patterns across observations and model ensembles, we here exploit the intrinsic similarities between the ocean's storage of heat and carbon.

Previous studies have shown that changes in global atmospheric surface temperatures are proportional to cumulative CO_2 emissions[1–3]. This emergent linear relationship is driven by the ocean, and the linearity arises in part from the ocean processes that are responsible for the uptake of heat and carbon[4,18] ('uptake' is the absorption of atmospheric anomalies by the ocean, and 'storage' is how these anomalies are stored spatially in the ocean). The result highlights a salient connection between the uptake and storage of heat and carbon in the ocean, setting the transient climate response to CO_2 emissions. Our study aims to quantify how changes in ocean processes and ocean circulation affect the ocean storage of heat and carbon at global and regional scales and we use our findings to establish the origin of ocean warming patterns.

On the global scale, we find that the ratio of heat to carbon uptake by the ocean spans a narrow range across observations, models and scenarios. On the regional scale, patterns of ocean heat and carbon storage are identical if ocean circulation—where 'circulation' herein refers to resolved advection (see below)—is unaltered by anthropogenic climate change, in both a coupled[7] and an ocean-only model. We use

[1]Atmospheric, Oceanic and Planetary Physics, University of Oxford, Oxford, UK. [2]Geophysical Fluid Dynamics Laboratory, Princeton, NJ, USA. [3]Department of Geosciences, University of Arizona, Tucson, AZ, USA. [4]Program in Atmospheric and Oceanic Sciences, Princeton University, Princeton, NJ, USA. [5]Courant Institute of Mathematical Sciences, New York University, New York, NY, USA. ✉e-mail: benjamin.bronselaer@cantab.net

Article

these two findings to attribute changes in the patterns of ocean heat storage to ocean circulation changes in an ensemble of coupled climate models and also in observations. We find that circulation changes have a dominant effect on observed heat storage patterns. However, the effect of circulation changes on the patterns of ocean heat storage diminishes as the climate warms over the twenty-first century.

To obtain our results, we initially use two 100-yr-long simulations of the Geophysical Fluid Dynamics Laboratory Earth System Model 2 (GFDL ESM2M) forced with a transient increase of 1% atmospheric CO_2 per year[7] (the 1%CO_2 experiment; see Methods). We analyse the results at the time of doubling of atmospheric CO_2, averaged over years 61–80 of the simulation. One simulation allows ocean currents to evolve freely (the free-circulation experiment) and the other prescribes monthly mean horizontal Eulerian velocities (ocean currents) from a pre-industrial control simulation (the fixed-circulation experiment), removing changes in ocean circulation induced by CO_2 forcing. Throughout this text, we define circulation as the advection by Eulerian velocities only—we therefore do not include parametrizations such as eddy velocities and mixing, which are allowed to vary in the fixed-circulation experiment. However, the changes in the eddy transport and convection in the fixed-circulation experiment are small, except in ice-covered regions (see Extended Data Fig. 1).

As a result of increased CO_2 forcing, excess energy in the climate system is mainly stored in the ocean. In our numerical experiments, the ocean heat storage in the fixed-circulation experiment—the added heat, H_{ad}—represents the storage of excess atmospheric heat as a result of pre-industrial ocean circulation and the changes in sub-grid processes (mixing and mesoscale eddies) owing to increased CO_2 forcing. The ocean heat storage in the free-circulation experiment, H, additionally includes the effect of circulation changes. The difference between the total heat storage H and the added heat H_{ad}, (both owing to anthropogenic climate change), here defined as the redistributed heat, H_r, is thus the redistribution of both the added and pre-industrial (background) heat throughout the ocean by the changing ocean circulation:

$$H = H_{ad} + H_r \tag{1}$$

Heat redistribution from circulation changes can strongly alter regional patterns of heat storage[5,8,10], and local climate feedback such as from clouds and albedo[7]; however, heat redistribution has little effect on global anthropogenic ocean heat uptake: the difference in global ocean heat uptake between the fixed-circulation and free-circulation experiments is only 4% in ESM2M[7] (this could vary slightly from model to model). A decomposition similar to equation (1) can be applied to any tracer anomaly in the ocean, including the anthropogenic ocean carbon storage, C_{ant}. We here refer to 'anthropogenic' heat and carbon as the anomalies from the pre-industrial state induced by increased atmospheric CO_2 concentration. All anomalies are calculated using 20-yr temporal averages to minimize the effects of natural variability. Given that heat and carbon anomalies are concentrated in the upper ocean[6,7,10], and for comparison with observations, we focus on the top 2,000 m vertically integrated fields. To verify our results from ESM2M, we also conduct similar simulations in an ocean-only model, here the Massachusetts Institute of Technology General Circulation Model (MITgcm), with free-circulation and fixed-circulation experiments, discussed in Methods.

Heat and carbon storage in GFDL ESM2M

In our ESM2M 1%CO_2 simulations, C_{ant} is concentrated in the mid and high latitudes, and is similar in both the free-circulation and fixed-circulation experiments, with a spatial correlation coefficient (CR) of 0.98 (Fig. 1a, b). The ocean redistribution of C_{ant} is negligible compared to the total C_{ant} (ref. [7]). The added heat in the fixed-circulation experiment is also predominantly stored in the mid and high latitudes

(Fig. 1e). In the fixed-circulation experiment, added heat is absorbed by the ocean as a result of air–sea exchange and is transported in the interior by background circulation and sub-grid processes. This heat storage H_{ad} is dominated by physical processes such as Ekman pumping and vertical mixing, and is heavily influenced by the pre-industrial stratification[19,20]. However, in the free-circulation experiment, there is noticeably more heat stored in the low latitudes of the Atlantic Ocean compared to in the fixed-circulation experiment, owing to the changing circulation (Fig. 1d)—either a change in gyre transport or overturning circulation[10,17]. Redistribution of heat (H_r) from the changing circulation is evident in all ocean basins, not just the Atlantic Ocean. The patterns of C_{ant}, in the free-circulation and the fixed-circulation experiments, closely match H_{ad}, with CRs of 0.92 and 0.93, respectively. Additionally, this similarity is evident in ocean-only MITgcm simulations, and also evident when comparing reconstructions of ocean heat and carbon storage using a constant ocean circulation[10,21].

The similarity of C_{ant} and H_{ad} is due to the effect of chemistry on ocean carbon uptake, through the Revelle buffer factor[22]. The spatial pattern of the buffer factor is largely determined by the pattern of the background ocean temperature (see Methods). By contrast, ocean uptake of other tracers such as chlorofluorocarbon (CFC) lacks chemical buffering, such that the ocean CFC storage does not have the same relationship with H_{ad} as C_{ant} does; H_{ad} and C_{ant} therefore have a unique similarity (see Methods for a detailed analysis).

Global heat–carbon coupling

Owing to the unique similarity between the spatial patterns of storage of C_{ant} and H_{ad} in the simulations, the spatial pattern of H_{ad} can be reconstructed using C_{ant} in the free-circulation experiment, without the need for a fixed-circulation experiment. To reconstruct H_{ad}, we require an appropriate time-varying scaling parameter, $\alpha(t)$, such that $H_{ad} = \alpha(t)C_{ant}$. Here, the coefficient α is called the heat–carbon coupling parameter. α can be estimated locally using a regression of C_{ant} onto H_{ad}, although this still requires a fixed-circulation experiment. Although the patterns of ocean heat storage differ between the free-circulation and fixed-circulation experiments, the global integrals of anthropogenic heat and carbon content are nearly unchanged (Fig. 2a)[7]. Therefore, we opt to estimate α globally such that

$$\alpha(t) = \frac{\int H(x, y, t)\,dA}{\int C_{ant}(x, y, t)\,dA} = \frac{\hat{H}(t)}{\hat{C}_{ant}(t)}, \tag{2}$$

where $\hat{H}$ and $\hat{C}_{ant}$ are the global spatial integrals of H and C_{ant}, respectively, and A is the surface area of the Earth. The value of α is generally in the range 2×10^7–6×10^7 J mol^{-1} when calculated for different model simulations, scenarios and observations (Fig. 2a). This relatively narrow range of values for α represents a tight coupling between the global ocean anthropogenic uptake of heat and carbon in the climate system.

To understand the leading terms that set the magnitude of α, denoted as $\tilde{\alpha}$, we consider how atmospheric CO_2 changes drive the anthropogenic ocean uptake of heat and carbon. Using the analytic expressions for the dependence of $\hat{H}$ and $\hat{C}_{ant}$ on atmospheric CO_2 (derived in Methods), we can express $\tilde{\alpha}$ as a function of simple parameters of the Earth system. We assume that ocean warming $\hat{H}$ is driven by the radiative forcing imbalance that stems from the strength of CO_2 as a greenhouse gas, F_0 (in W m^{-2}). In addition, we assume that changes in ocean carbon uptake are directly driven by excess atmospheric CO_2 concentration and that C_{ant}, the amount of anthropogenic carbon absorbed by the ocean, is set by the capacity of the ocean to buffer CO_2 anomalies, expressed by the Revelle buffer factor[4,22], R_{DIC} (DIC, dissolved inorganic carbon). A lower value of R_{DIC} and a higher total ocean carbon inventory I_0 can both contribute to a lower capacity for the ocean to absorb additional CO_2. We combine the relationships for the uptake of ocean heat
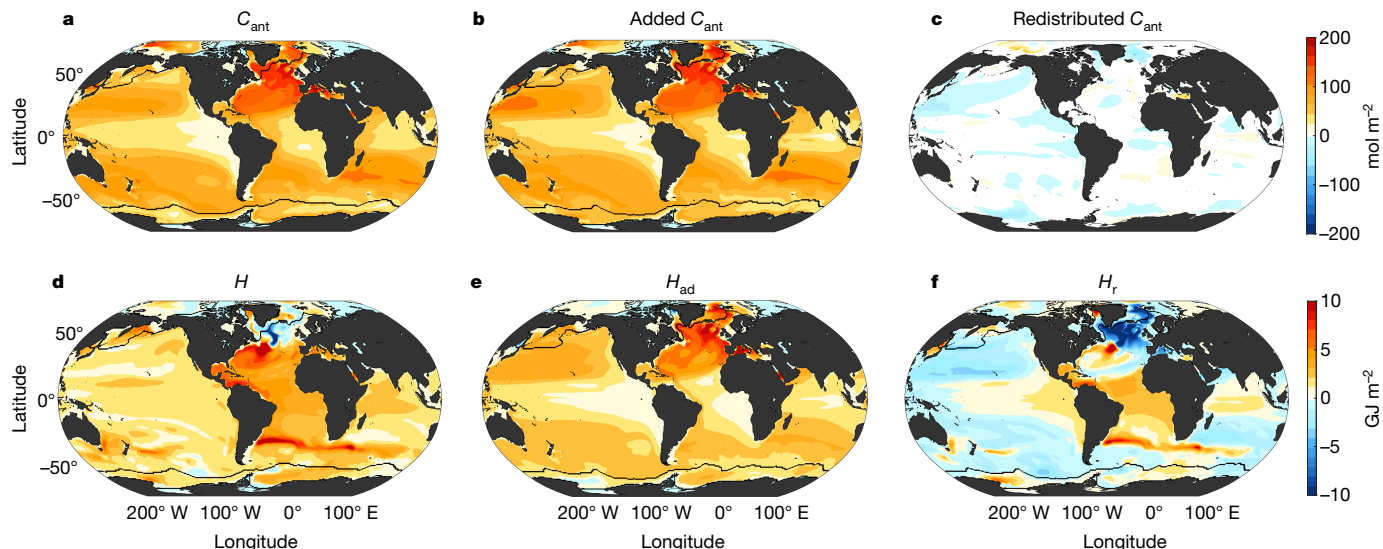
Fig. 1 | Simulated anthropogenic changes in C_{ant} and H. a–f, Upper 2,000 m vertically integrated anomalies in years 61–80 of the 1%CO_2 ESM2M simulation for tracers C_{ant} (**a–c**) and H (**d–f**). **a, d**, C_{ant} and H relative to the tandem control simulation for the free-circulation experiment. **b, e**, Added C_{ant} and added H (H_{ad}) relative to the tandem control simulation fixed-circulation experiments. **c, f**, The difference in C_{ant} and H between the free-circulation and fixed-circulation experiments, which is attributed to the changing ocean currents—that is, the redistributed values of C_{ant} and H (that is, H_r). The black line shows the annual-mean maximum sea-ice extent.

and carbon and, by neglecting climate feedback, we obtain an expression for $\tilde{\alpha}$ given by (see Methods):

$$\tilde{\alpha}(t) \approx A \frac{R_{DIC} F_0}{I_0} \Delta t, \qquad (3)$$

where Δt is the time interval elapsed (see Methods for further details). In ESM2M, the estimated α ($\tilde{\alpha}$) determined by equation (3) is of similar magnitude to the directly obtained α (equation (2)), particularly after the first 20 yr of simulations (during which time natural variability dominates over the anthropogenic response; see Extended Data Fig. 2 and Methods). However, after a few decades, observations and models show little temporal dependence on α (Fig. 2b and Extended Data Fig. 2), probably owing to the importance of the feedback processes that are neglected in equation (3). The observed and modelled constant slope of $\hat{H}$ versus $\hat{C}_{ant}$—that is, α (Fig. 2b)—therefore highlights that the ocean takes up heat at the same rate as it takes up carbon. This relationship is similar to the linear relationship between atmospheric warming and cumulative carbon emissions. Thus we determine that, to first order, the linear relationship between the global uptake of heat and carbon is determined by the capacity of the ocean to take up carbon and the strength of the radiative forcing of CO_2.

Past and future heat redistribution

By exploiting this relationship between global heat and carbon uptake, H_{ad} can be locally reconstructed from C_{ant} using $H_{ad}(x,y,t) = \alpha(t) C_{ant}(x,y,t)$, where $\alpha(t)$ (equation (2)) is obtained for each individual simulation or observational product. The global-mean error in ice-free regions for the estimated H_{ad} over the upper 2,000 m of the ocean, compared to the simulated H_{ad} in ESM2M, is 11%. We obtain similar errors using different depth integrals (shown in Fig. 3) or using an ocean-only model (see Methods). We can then infer vertically integrated patterns of redistribution, $H_r(x,y,t)$, as residuals using equation (1). The reconstruction of depth-dependent profiles of zonal-mean heat redistribution is just as accurate below 300 m (Extended Data Fig. 3).

We apply our method to observational products using spatially and temporally varying ocean heat storage (from ref. [23]) and anthropogenic

carbon (from ref. [24]), from 1951 to 2011 in the top 2,000 m of the ocean. The storage of anthropogenic heat and carbon is calculated by fitting linear trends locally over the period, multiplied by the time period considered (Fig. 4). We apply the same procedure to 11 Earth system models from the CMIP5 archive with a full carbon cycle. Although there is a large inter-model spread in historical ocean heat storage among CMIP5 simulations (±71%), the CMIP5 ensemble mean agrees well with observations of net global ocean heat storage over the past 40 yr[11]. We use historical and climate change simulations (following the Recommended Concentration Pathway 8.5, RCP8.5) for 1951–2011 and 2011–2060, respectively. We also reconstruct projections of redistributed heat using the 2011–2060 trends from CMIP5 in the RCP8.5 simulations (Fig. 4).

Overall, the CMIP5 models reproduce the observed 1951–2011 added heat storage better than they do the redistributed heat storage; the CR for the observed and simulated mean H_{ad} is 0.83, whereas the CR for observed and simulated H_r is 0.31. However, some features in the spatial patterns of H_r over 1951–2011 are consistent between observations and the CMIP5 simulations, as well as in our ESM2M 1%CO_2 simulation; for example, cooling in the Pacific sub-tropical gyres and the Indian Ocean, and warming in the tropics. However, the ensemble mean of the CMIP5 simulations underestimates the strength of tropical redistributed warming compared to the observations, especially in the Atlantic Ocean. This is partly due to inter-model variability. In the Southern Ocean, the observed patterns of warming show substantial contributions from added heat in all three sectors of the Southern Ocean: large redistributed warming in the Atlantic and Indian sectors, and weak cooling in the Pacific sector. The zonally integrated heat storage in the Southern Ocean is dominated by the added heat[25], owing in part to the integration both over the redistributed warming anomalies (in the Atlantic and Indian sectors of the Southern Ocean) and also over the cooling anomalies (in the Pacific sector). The CMIP5 models simulate more redistributed cooling in the Pacific sector of the Southern Ocean compared to observations over the same period, but simulate a weaker redistributed warming feature in the Atlantic and Indian sectors, seen also in the Atlantic zonal mean (see Extended Data Fig. 4).

A key feature of H_r inferred from the observations is the cooling effect of the redistributed heat in the North Atlantic subpolar gyre, consistent
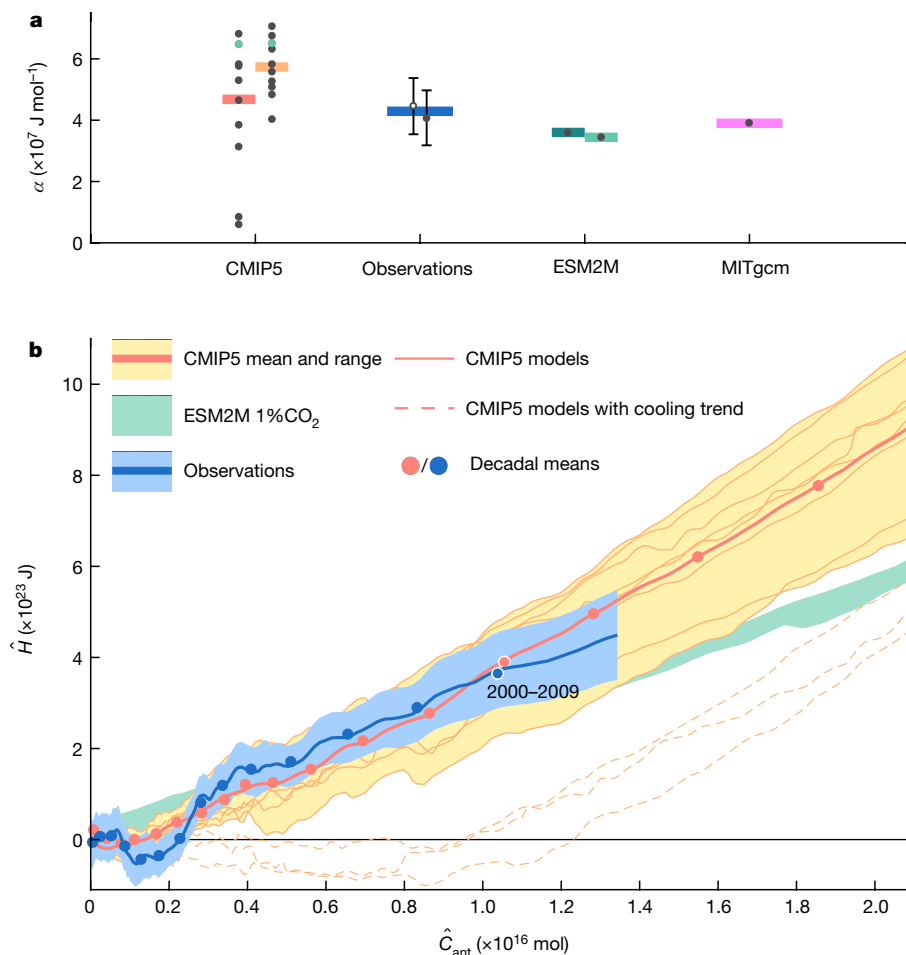
Fig. 2 | Heat–carbon coupling. a, α calculated from (left to right): the 1951–2011 trend in the CMIP5 ensemble historical simulations (ensemble mean in red); the 1951–2060 trend in the CMIP5 ensemble RCP8.5 simulation (ensemble mean in orange); the 1951–2011 trend in observations of ocean heat content (white circle from ref. [10], filled circle from ref. [23]), and in observations of ocean carbon content[24] (mean, blue); our ESM2M 1%CO_2 model after 70 yr of the fixed-circulation (dark green) and free-circulation (light green) experiments; and from the perturbed MITgcm simulation after 70 yr (magenta). The grey dots show individual estimates; the green circles show ESM2M within the CMIP5 ensemble. The error bars show the 66% confidence interval stemming from the combined observational uncertainty in H and C_{ant}. **b**, $\hat{H}$ as a function of $\hat{C}_{ant}$ relative to the years 1870–1890, where the slope is equal to α. The CMIP5 historical-RCP8.5 ensemble members are given up to the year 2060, where the ensemble mean is the thick solid pink line, the range is shaded in pale yellow and the thin solid pink lines show individual models. The dashed lines show the CMIP5 models that simulate a decrease in the ocean heat content in the twentieth century, which are excluded from the mean and range. The blue line shows observations (ocean heat storage from ref. [10]), and the green shading shows the range of the fixed-circulation and free-circulation 1%CO_2 ESM2M simulations that we conduct here. The solid circles show the decadal means, and the white rings highlight the 2000–2009 mean. The blue shading shows the 66% confidence interval from observations.

with a reduction in the meridional ocean heat transport that is probably due to a reduction in the meridional overturning circulation or gyre transport[10,17], which counteracts the warming from the added heat. This North Atlantic redistribution is not captured in the CMIP5 ensemble mean but is present in a few of the ensemble members (Extended Data Fig. 5). This could indicate either that the sub-polar cooling is due to natural variability (an anthropogenic signal in meridional heat transport only emerged in 2000)[26] and therefore eliminated owing to the averaging over multiple historical simulations, or that most CMIP5 ESM models fail to capture the emergence of a forced trend in that region because they contain structural biases[27].

In our projections from 2011 to 2060, in all CMIP5 models—including in the three CMIP5 models that best match the observed patterns of H_r from 1951 to 2011—H_r exhibits a cooling signal in the Atlantic sub-polar gyre and warming in the Gulf Stream and in low-latitude regions (Extended Data Fig. 5). This agreement could indicate that the observed pattern of ocean redistribution from anthropogenic climate change might persist over the coming decades, despite the past influence of natural variability. However, it is important to note that model agreement does not necessarily mean that the models are correct.

Heat redistribution explains most of the warming pattern over the historical period—H_r has a CR of 0.92 with H in observations (CR = 0.87 in CMIP5). However, the projected added heat becomes relatively more important between 2011 and 2060, with a CR of 0.52 for H_{ad} with H, as opposed to CR = 0.27 in observations and CR = 0.26 in CMIP5 over the historical period. As the climate warms, added heat storage will therefore probably begin to shape ocean warming patterns.

Discussion

We identify an emergent coupling between the global ocean uptake of heat and carbon. The order of magnitude of the heat–carbon coupling parameter is consistent across models, scenarios and observations and is mostly constant over time. The magnitude of the heat–carbon coupling parameter is, to first order, set by the ocean buffer factor,
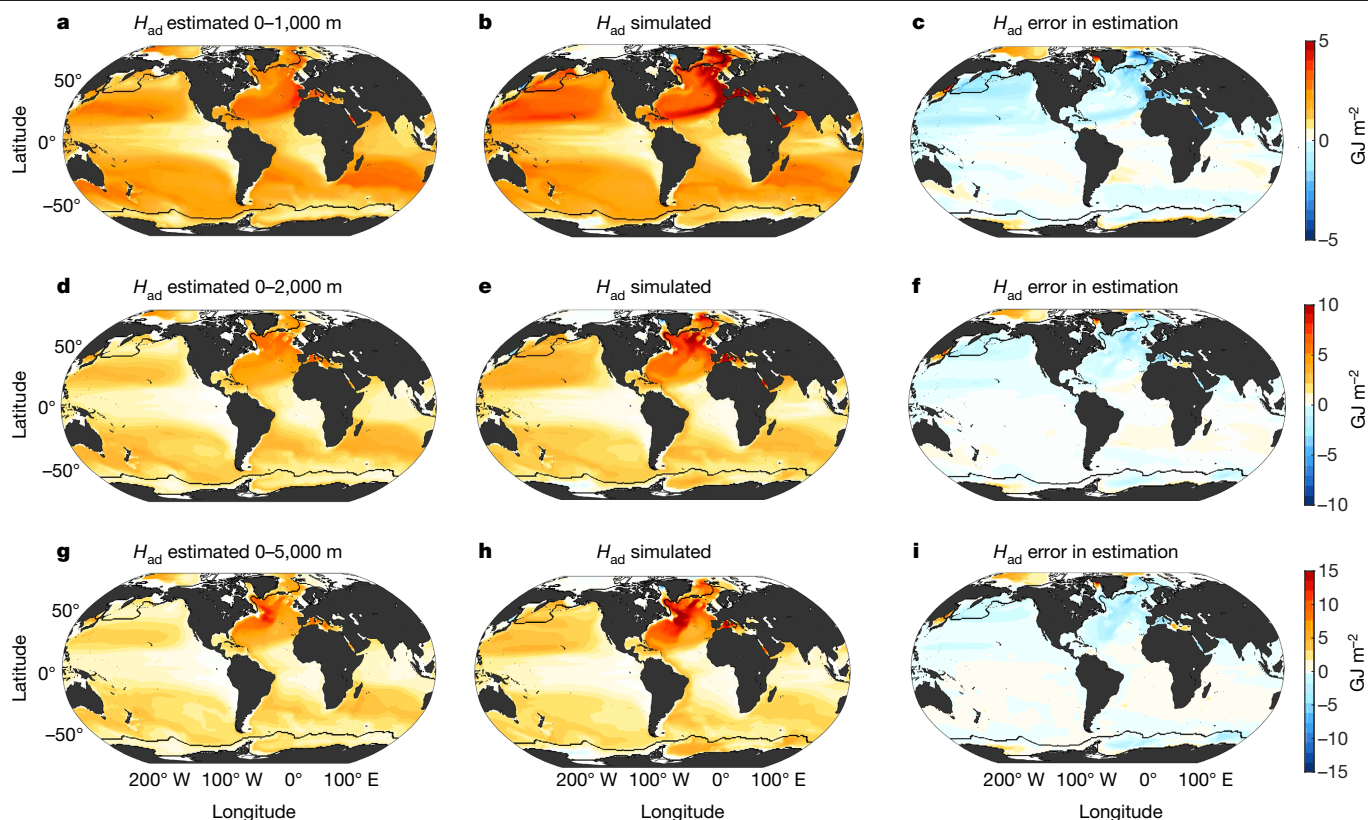
Fig. 3 | Error in the redistributed ocean heat storage from ESM2M.
a–**i**, Ocean heat storage from the fixed-circulation experiment in terms of the added H (H_{ad}), depth-integrated over 0–1,000 m (**a**–**c**), 0–2,000 m (**d**–**f**), and 0–5,000 m (**g**–**i**), averaged over years 61–80 of the ESM2M 1%CO_2 simulation. **a**, **d** and **g** show H_{ad} estimated using only the free-circulation experiment

quantity αC_{ant}, and **b**, **e** and **h** show H_{ad} simulated by the fixed-circulation experiment. **c**, **f** and **i** show the difference between H_{ad} as determined by the two experiments. The average percentage errors in the estimation of H_{ad} using C_{ant} are 3%, 11% and 12% for the models over 0–1,000 m, 0–2,000 m and 0–5,000 m, respectively.

the pre-industrial ocean carbon inventory and the radiative forcing strength of CO_2. This similarity is unique in that it is not shared with other passive tracers such as ocean CFC storage. We use the global and regional coupling of heat and carbon to calculate patterns of the ocean heat redistribution that arises from circulation changes in observational-based products and in CMIP5 models from 1951 to 2060.

The method allows us to attribute observed ocean warming and cooling to circulation changes on a global scale using only observational products, thereby avoiding the biases in climate models that are associated with their simulated heat-storage patterns. In some ocean basins, the effect of warming from redistribution is more than three times larger than the effect of added heat storage in the fixed-circulation experiment, leading to an increased rise in regional sea levels. We find that warming from redistribution has had an important role in the observed warming of the Atlantic Ocean between 40° S and 40° N and in the eastern tropical Pacific Ocean, up to 6.4 GJ m^{-2} along the Gulf Stream. In contrast to warming from redistribution, changes in ocean circulation have probably cooled the sub-tropical gyres in both the Indian and Pacific Oceans by up to 2.4 GJ m^{-2}, leading to mitigation of local sea-level rise. In the Southern Ocean, there is redistributed warming in the South Atlantic and Indian sectors, up to 4.0 GJ m^{-2}, but cooling in the Pacific sector, up to 1.7 GJ m^{-2}, such that the zonally integrated Southern Ocean warming is set by the added heat[25]. Over the historical period, some of these observed features are probably due to natural variability. However, both the Pacific and Indian sub-tropical redistributed cooling and Southern Ocean pattern are projected to continue into the future across all models[8], suggesting that the historical pattern of redistribution may persist over the next several decades.

Simulations of the storage of ocean anthropogenic carbon—and by extension the added heat storage—within the CMIP5 ensemble agree well with each other[28]. Therefore, the differences in heat-storage patterns simulated in the CMIP5 models are not due to the background state, which governs the added heat storage, but are predominantly due to the response of the ocean circulation to forcing in these models (natural or anthropogenic). In future projections, however, the influence of ocean heat redistribution on patterns of heat storage is reduced as the added heat becomes more dominant, despite changes in ocean circulation becoming more severe[29]. In addition, the patterns of added heat storage in CMIP5 models agree well with observations. As added heat storage becomes more dominant, future CMIP simulations of ocean heat storage will therefore probably agree better with real patterns of warming than in the past. As a result, long-term ocean warming and patterns of sea-level rise may become more predictable as the climate warms. However, we cannot exclude that at even higher atmospheric CO_2 levels than tested here, extreme and abrupt changes in circulation may have an important role.

A main caveat of our work is the use of a single coupled climate model (ESM2M) to test our method. However, all key results found using ESM2M are also found in ocean-only simulations with MITgcm. In the MITgcm simulations, we also find a 4% difference in global heat uptake between the fixed-circulation and free-circulation experiments after 100 yr of simulation, that the redistribution of C_{ant} is negligible, that patterns of carbon and heat storage in the fixed experiment are highly correlated, that α lies in the range of other coupled models, and that all of these results can be used to skilfully reconstruct fixed heat storage (see Methods). In addition, both the spatial similarity of C_{ant}
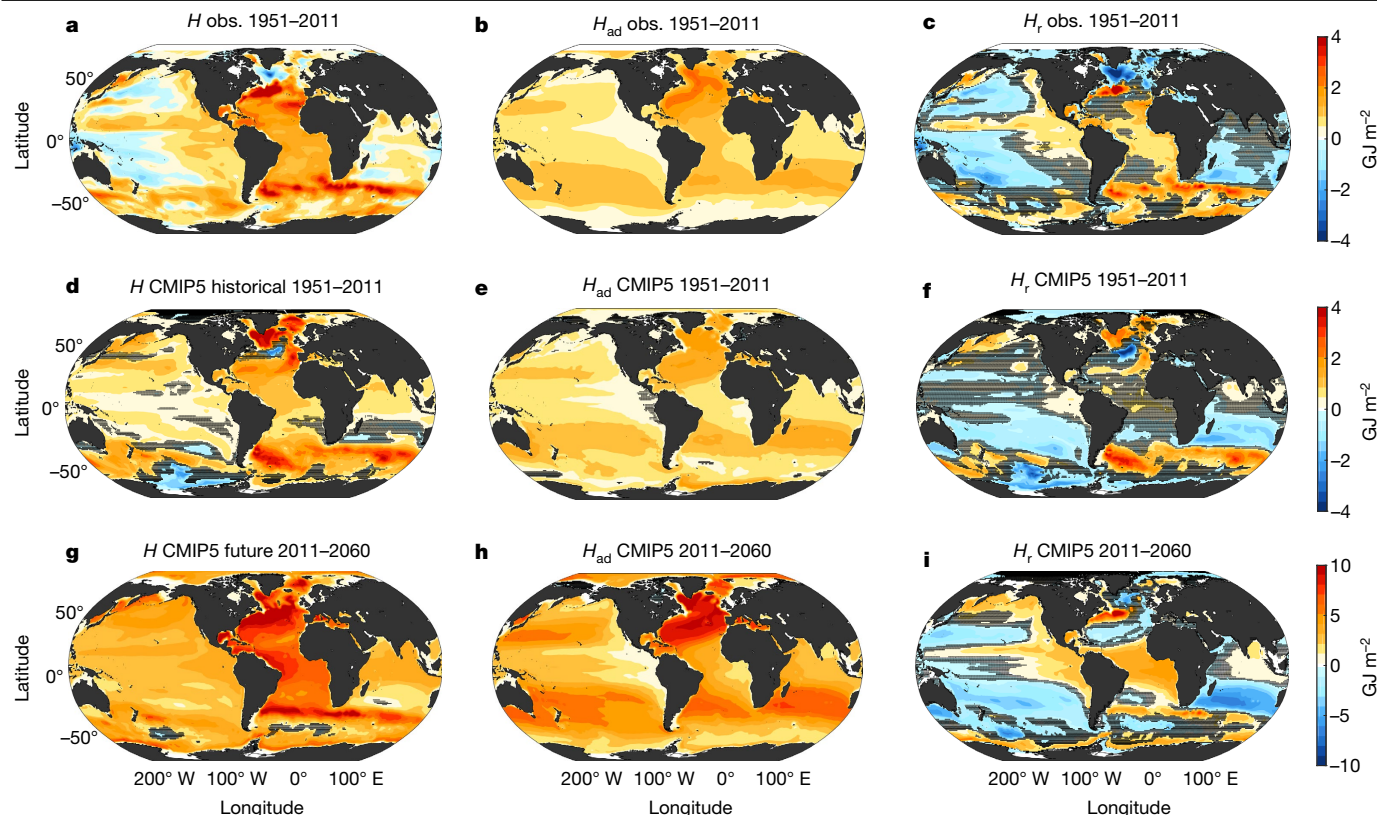
a, **d**, **g**, The change in heat storage *H*. **b**, **e**, **h**, The change in the added heat storage H_{ad}, calculated as αC_{ant}. **c**, **f**, **i**, The ocean redistributed heat $H_r = H - \alpha C_{ant}$. The changes are shown as the linear trends over the indicated periods multiplied by the length of the period. The results from observational estimates (obs.) for the period 1951–2011 are given in **a**–**c**; the results from

Fig. 4 | Redistribution of ocean heat storage in the upper 2,000 m. 1951–2011 changes in the CMIP5 historical-RCP8.5 ensemble are given in **d**–**f**; and **g**–**i** show the 2011–2060 changes in the CMIP5 RCP8.5 ensemble. The hatching indicates where the changes are not significant at the 66% uncertainty level. For the observations, the uncertainty is from the estimates of *H* and C_{ant}, whereas for the CMIP5 models, the uncertainty is from the mean of the ensemble that emerges from the inter-model spread.

under free-circulation and fixed-circulation conditions[6,21], and also the small effect of biological changes[6,21,30–32] on C_{ant} are consistent with previous modelling work. In the fixed-circulation experiment, parameterizations are still allowed to vary. However, the effect of changes in these parameterizations on the passive heat and carbon storage is found to be less than 10% (see Methods). Finally, the similarity between H_{ad} and C_{ant} is also present when comparing passive reconstructions of the storage of ocean heat and carbon[10,21]. Another caveat of our work is that many models tend to underestimate variability, including air–sea carbon fluxes[33,34]. However, because we consider the multi-decadal time-integrated carbon storage, the effects of variability in the flux are mostly mitigated.

In summary, we present a method to calculate the redistribution of ocean heat without the need for any additional measurements or simulations, and we infer changes in heat transport owing to anthropogenic climate change. The method provides a way to assess the quality of climate models, by comparing the physical response to forcing with our observational estimate of ocean heat redistribution. We show that ocean heat redistribution, although dominant in the past, becomes less important in the future, leading to potentially more predictable warming patterns in coarse-resolution climate models. Further work is necessary to assess our results in eddy-rich ocean climate models, and to constrain the mechanisms and sensitivity of ocean heat to carbon uptake and their potentially strong link to the transient climate response to CO_2 emissions[1]. However, our method can be used to understand the mechanisms which regionally redistribute ocean heat, impacting sea-ice formation[35], marine heat waves[36], ocean oxygen[37] and sea-level rise[10,38].

Online content

Any methods, additional references, Nature Research reporting summaries, source data, extended data, supplementary information, acknowledgements, peer review information; details of author contributions and competing interests; and statements of data and code availability are available at https://doi.org/10.1038/s41586-020-2573-5.

1. Allen, M. R. et al. Warming caused by cumulative carbon emissions towards the trillionth tonne. *Nature* **458**, 1163–1166 (2009).
2. Matthews, H. D., Gillett, N. P., Stott, P. A. & Zickfeld, K. The proportionality of global warming to cumulative carbon emissions. *Nature* **459**, 829–832 (2009).
3. Solomon, S., Plattner, G., Knutti, R. & Friedlingstein, P. Irreversible climate change due to carbon dioxide emissions. *Proc. Natl Acad. Sci. USA* **106**, 1704–1709 (2009).
4. Goodwin, P., Williams, R. G. & Ridgwell, A. Sensitivity of climate to cumulative carbon emissions due to compensation of ocean heat and carbon uptake. *Nat. Geosci.* **8**, 29–34 (2015).
5. Xie, P. & Vallis, G. K. The passive and active nature of ocean heat uptake in idealized climate change experiments. *Clim. Dyn.* **38**, 667–684 (2012).
6. Khatiwala, S. et al. Global ocean storage of anthropogenic carbon. *Biogeosciences* **10**, 2169–2191 (2013).
7. Winton, M., Griffies, S. M., Samuels, B. L., Sarmiento, J. L. & Frölicher, T. L. Connecting changing ocean circulation with changing climate. *J. Clim.* **26**, 2268–2278 (2013).
8. Gregory, J. M. et al. The Flux-Anomaly-Forced Model Intercomparison Project (FAFMIP) contribution to CMIP6: investigation of sea-level and ocean climate change in response to CO_2 forcing. *Geosci. Model Dev.* **9**, 3993–4017 (2016).
9. DeVries, T., Holzer, M. & Primeau, F. Recent increase in oceanic carbon uptake driven by weaker upper-ocean overturning. *Nature* **542**, 215–218 (2017).
10. Zanna, L., Khatiwala, S., Gregory, J. M., Ison, J. & Heimbach, P. Global reconstruction of historical ocean heat storage and transport. *Proc. Natl Acad. Sci. USA* **116**, 1126–1131 (2019).
11. Frölicher, T. L. et al. Dominance of the Southern Ocean in anthropogenic carbon and heat uptake in CMIP5 models. *J. Clim.* **28**, 862–886 (2015).

12. Stocker, T.F. et al. (eds) *Climate Change 2013: The Physical Science Basis: Contribution of Working Group I to the Fifth Assessment Report of the Intergovernmental Panel on Climate Change* (Cambridge Univ. Press, 2013).

13. Drijfhout, S., van Oldenborgh, G. J. & Cimatoribus, A. Is a decline of AMOC causing the warming hole above the North Atlantic in observed and modeled warming patterns? *J. Clim*. **25**, 8373–8379 (2012).

14. Wilson, L. J. et al. Climate-driven changes to ocean circulation and their inferred impacts on marine dispersal patterns. *Glob. Ecol. Biogeogr*. **25**, 923–939 (2016).

15. Smeed, D. A. et al. The North Atlantic Ocean is in a state of reduced overturning. *Geophys. Res. Lett*. **45**, 1527–1533 (2018).

16. Matear, R. J., Hirst, A. C. & McNeil, B. I. Changes in dissolved oxygen in the Southern Ocean with climate change. *Geochem. Geophys. Geosyst*. **1**, 1050 (2000).

17. Caesar, L., Rahmstorf, S., Robinson, A., Feulner, G. & Saba, V. Observed fingerprint of a weakening Atlantic Ocean overturning circulation. *Nature* **556**, 191–196 (2018).

18. Zickfeld, K., Eby, M., Matthews, H. D. & Weaver, A. J. Setting cumulative emissions targets to reduce the risk of dangerous climate change. *Proc. Natl Acad. Sci. USA* **106**, 16129–16134 (2009).

19. Marshall, D. P. & Zanna, L. A conceptual model of ocean heat uptake under climate change. *J. Clim*. **27**, 8444–8465 (2014).

20. Saenko, O. A., Yang, D. & Gregory, J. M. Impact of mesoscale eddy transfer on heat uptake in an eddy-parameterizing ocean model. *J. Clim*. **31**, 8589–8606 (2018).

21. Khatiwala, S., Primeau, F. & Hall, T. Reconstruction of the history of anthropogenic CO_2 concentrations in the ocean. *Nature* **462**, 346–349 (2009).

22. Revelle, R. & Suess, H. S. Carbon dioxide exchange between atmosphere and ocean and the questions of an increase of atmospheric CO_2 during the past decades. *Tellus* **9**, 18–27 (1957).

23. Cheng, L. et al. Improved estimates of ocean heat content from 1960 to 2015. *Sci. Adv*. **3**, e1601545 (2017).

24. DeVries, T. The oceanic anthropogenic CO_2 sink: storage, air–sea fluxes, and transports over the industrial era. *Glob. Biogeochem. Cycles* **28**, 631–647 (2014).

25. Armour, K. C., Marshall, J., Scott, J. R., Donohoe, A. & Newsom, E. R. Southern Ocean warming delayed by circumpolar upwelling and equatorward transport. *Nat. Geosci*. **9**, 549–554 (2016).

26. Chemke, R., Zanna, L. & Polvani, L. M. Identifying a human signal in the North Atlantic warming hole. *Nat. Commun*. **11**, 1540 (2020).

27. Huber, M. B. & Zanna, L. Drivers of uncertainty in simulated ocean circulation and heat uptake. *Geophys. Res. Lett*. **44**, 1402–1413 (2017).

28. Bronselaer, B., Winton, M., Russell, J., Sabine, C. L. & Khatiwala, S. Agreement of CMIP5 simulated and observed ocean anthropogenic CO_2 uptake. *Geophys. Res. Lett*. **44**, 12298–12305 (2017).

29. Cheng, W., Chiang, J. C. H. & Zhang, D. Atlantic Meridional Overturning Circulation (AMOC) in CMIP5 models: RCP and historical simulations. *J. Clim*. **26**, 7187–7197 (2013).

30. Friedlingstein, P. et al. Climate–carbon cycle feedback analysis: results from the C4MIP model intercomparison. *J. Clim*. **19**, 3337–3353 (2006).

31. Arora, V. K. et al. Carbon–concentration and carbon–climate feedbacks in CMIP5 Earth system models. *J. Clim*. **26**, 5289–5314 (2013).

32. Friedlingstein, P. et al. Uncertainties in CMIP5 climate projections due to carbon cycle feedbacks. *J. Clim*. **27**, 511–526 (2014).

33. Landschützer, P., Gruber, N. & Bakker, D. C. E. Decadal variations and trends of the global ocean carbon sink. *Glob. Biogeochem. Cycles* **30**, 1396–1417 (2016).

34. DeVries, T. et al. Decadal trends in the ocean carbon sink. *Proc. Natl Acad. Sci. USA* **116**, 11646–11651 (2019).

35. Winton, M. On the climatic impact of ocean circulation. *J. Clim*. **16**, 2875–2889 (2003).

36. Frölicher, T. L., Fischer, E. M. & Gruber, N. Marine heatwaves under global warming. *Nature* **560**, 360–364 (2018).

37. Palter, J. B. & Trossman, D. S. The sensitivity of future ocean oxygen to changes in ocean circulation. *Glob. Biogeochem. Cycles* **32**, 738–751 (2018).

38. Banks, H. & Gregory, J. Mechanisms of ocean heat uptake in a coupled climate model and the implications for tracer-based predictions of ocean heat uptake. *Geophys. Res. Lett*. **33**, L07608 (2006).

Article

Methods

Experimental design

The main coupled climate model used in this study is the GFDL ESM2M, which includes a fully coupled carbon cycle[39,40] forced with a transient increase of 1% atmospheric CO_2 per year[7]. To investigate the effect of changing currents, in addition to a free-running forced experiment, we use the fixed-circulation experiments from ref. [7]. In these experiments, the ocean currents (namely, the horizontal velocities) are prescribed to follow a fixed seasonal cycle. The prescribed (fixed) currents are taken from the first 100 yr of the 1860 control simulation. To maintain the mass balance and avoid unrealistic local sea levels, the ocean surface freshwater flux in the 1%CO_2 fixed-circulation experiment is also prescribed from the pre-industrial fixed-circulation control. Although the resolved currents are prescribed, the parameterizations for subgrid-scale mesoscale eddy mixing and convection are allowed to operate as normal and respond to the imposed CO_2 forcing.

The experiments are run for 100 yr but herein we show the spatial maps of anomalies over the years 61–80, which coincide with the time at which the atmospheric CO_2 concentration is twice the pre-industrial value. In the ESM2M simulations, the difference in the net ocean heat uptake for the average of the years 61–80 between the fixed-circulation and free-circulation simulations is 4%.

In the fixed-circulation experiment, there are some changes in the circulation owing to the eddy parameterization schemes (Gent–McWilliams and vertical mixing), shown in Extended Data Fig. 1. However, these changes are negligible. Extended Data Fig. 1 also shows the mixed layer depth in the control simulation and calculated changes in the mixed layer depth in the free-circulation and fixed-circulation experiments. Changes in the mixed layer depths reflect changes in convection. Although there are large changes in mixed layer depths in the free-circulation experiment in the North Atlantic (particularly in the Labrador Sea), there are only small changes in the ice-free regions of the fixed-circulation experiment, where convection is maintained. In the fixed-circulation experiment, in the North Atlantic north of 30° N, there is an average reduction in the mixed layer depth of 13%, where mixed layer depths were deeper than 200 m in the control case. These results show that, outside ice-covered regions, the changes in the eddy and convection parameterizations in the fixed-circulation experiment are small.

Similarity between C_{ant} and H_{ad}

To demonstrate the similarity between C_{ant} and H_{ad}, we investigate the relationship between heat and CFC storage from an RCP8.5 simulation, also at the time of the doubling of the atmospheric partial pressure of CO_2, p_{CO_2} (Extended Data Fig. 6). Ocean uptake of atmospheric CO_2 is driven by the air–sea imbalance of the partial pressure of CO_2. At the ocean surface, changes in p_{CO_2} are largely latitudinally uniform[41,42] (Extended Data Fig. 6), which is a result of surface waters being mostly equilibrated with respect to well-mixed atmospheric CO_2[43,44]. Changes in ocean p_{CO_2}, Δp_{CO_2}, therefore follow the nearly latitudinally uniform atmospheric CO_2 changes, imposing a strong constraint on the pattern of surface p_{CO_2}.

p_{CO_2} can be decomposed as the change in p_{CO_2} from temperature changes ΔT, and changes owing to chemistry, using linearity and the chain rule. In this case, we can express the contribution of chemistry through the changes in concentrations of DIC, ΔDIC, and of alkalinity (ALK), ΔALK:

$$\Delta p_{CO_2}(T, \text{DIC}, \text{ALK}, S) \approx \frac{\partial p_{CO_2}}{\partial T}\Delta T + \frac{\partial p_{CO_2}}{\partial \text{DIC}}\Delta \text{DIC} + \frac{\partial p_{CO_2}}{\partial \text{ALK}}\Delta \text{ALK}, \quad (4)$$

where the contribution from changes in salinity is negligible compared to the other factors[45] in equation (4). The ΔDIC term dominates Δp_{CO_2}

(Extended Data Fig. 6). Using the following expressions for the buffer factors for DIC and alkalinity (ALK), R_{DIC} and R_{ALK}, respectively[45,46]:

$$R_{DIC} \approx \frac{3 \times \text{ALK} \times \text{DIC} - 2 \times \text{DIC}^2}{(2 \times \text{DIC} - \text{ALK})(\text{ALK} - \text{DIC})}, \quad (5)$$

$$R_{ALK} \approx \frac{\text{ALK}^2}{(2 \times \text{DIC} - \text{ALK})(\text{ALK} - \text{DIC})}, \quad (6)$$

and an empirically derived relationship[47] for $\partial p_{CO_2}/\partial T$, we can rewrite equation (4) as follows:

$$\begin{aligned} p_{CO_2}(T, \text{DIC}, \text{ALK}) = 0.0423 p_{CO_2}\Delta T + \frac{R_{DIC}p_{CO_2}}{\text{DIC}}\Delta \text{DIC} \\ + \frac{R_{ALK}p_{CO_2}}{\text{DIC}}\text{DIC} + \frac{R_{ALK}p_{CO_2}}{\text{ALK}}\text{ALK}. \end{aligned} \quad (7)$$

The sensitivity $\partial p_{CO_2}/\partial \text{DIC}$ is set by the background ocean chemistry[22], the spatial pattern of which is partly determined by the background ocean temperature, as shown in Extended Data Fig. 6. To determine the role of temperature on $\partial p_{CO_2}/\partial \text{DIC}$, we remove latitudinal variations in temperature: we first calculate the pre-formed DIC (that is, C_{SAT}, the component of DIC that is in equilibrium with atmosphere, and the solubility of which is determined by temperature and salinity)[48] in the case of DIC. The pre-formed DIC was calculated twice, first using the simulated spatially varying background temperature field, and then using a uniform temperature field. The difference between the two is then removed from the actual simulated DIC to remove the effects of the spatially varying temperature. p_{CO_2} is also calculated with the same simulated and uniform temperature field, and the difference is used to remove the effects of the spatially varying temperature field.

To satisfy the latitudinally uniform surface Δp_{CO_2} constraint, ΔDIC must be anti-correlated to $\partial p_{CO_2}/\partial \text{DIC}$; in the ESM2M, CR = −0.84, with similar correlations in other models and observations (Extended Data Fig. 7). The patterns of ΔDIC, which are dictated by $\partial p_{CO_2}/\partial \text{DIC}$ and therefore by the background state, are similar in both the fixed-circulation and free-circulation experiments (CR = 0.98), as expected.

The patterns of ΔDIC are also found to correlate with the temperature change in the fixed-circulation experiment (that is, the added temperature ΔT_{ad}; CR = 0.64), and with the background temperature (CR = 0.8). However, concentration changes of CFCs are not strongly correlated with ΔT_{ad}. Similar to CO_2, the ocean uptake of CFCs is set by the air–sea imbalance in partial pressure of CFC, p_{CFC}, but unlike CO_2, CFCs lack chemical buffering and the surface p_{CFC} is only related to the CFC concentration by the inverse of solubility[49], and the lack of chemical buffering of CFCs breaks the correlation between CFC changes and ΔT_{ad}.

Once carbon and heat anomalies are absorbed by the ocean at the surface, the interior C_{ant} and H_{ad} patterns are set only by the background physical processes, with little impact from changes in sub-grid processes, as illustrated using a 'fixed-climate simulation'[30] in which atmospheric CO_2 has no radiative forcing effect. In this simulation, the ocean only sees a pre-industrial climate, without physically driven changes in temperature and ocean circulation. Between the fixed-climate ESM2M simulation and the fixed-circulation and free-circulation simulations, C_{ant} is almost identical (Extended Data Fig. 8), confirming that temperature and circulation changes have negligible effects on C_{ant}[28]. The fixed-climate simulation also shows that changes in biology have little effect, because modelled biological changes are primarily driven by physical changes in stratification that do not occur in the fixed-climate simulation[50–52]. Lastly, parameterizations such as convection, mixing and eddy transports are unperturbed in the fixed-climate simulation. The difference in C_{ant} between the fixed-climate and fixed-circulation

experiments is less than 10% locally. These simulations therefore also show that the parameterizations have only a small effect on passive tracer storage and are consistent with results from previous studies with other CMIP5 models[21,53,54].

The correlation between ΔDIC and fixed-circulation ΔT_{ad} at the surface owing to chemical buffering, as well as the dominance of background physical processes in setting H_{ad} and C_{ant} explain their strong correlation. By contrast, the lack of correlation between changes in surface CFC and ΔT_{ad} leads to a mismatch in storage patterns (Extended Data Fig. 6). CFCs therefore cannot be used to reconstruct H_{ad}, whereas C_{ant} uniquely can.

Relationship between global ocean anthropogenic heat and carbon

This section outlines a more detailed derivation of equation (3). We express the top-of-the-atmosphere radiative imbalance[55], $N(t)$, as the imbalance between the radiative forcing from CO_2, $F(t)$, and the climate feedback, $\lambda(t)T_a(t)$, such that:

$$N(t) = F(t) - \lambda(t)T_a(t) = \frac{\hat{H}(t)}{A\Delta t}, \tag{8}$$

where $\hat{H}(t)$ is the global heat uptake $\hat{H}$ since $t = 0$, Δt is the time interval elapsed, A is the surface area of the Earth, $T_a(t)$ is the mean atmospheric warming and $\lambda(t)$ is the climate sensitivity parameter. Note that in effect, $\Delta t = t$, but we use this notation to make it clear when a quantity is evaluated at a time t, and when the time elapsed appears as a separate quantity Δt. Most of the excess heat is absorbed by the ocean such that $A \times N(t) \approx \hat{H}(t)/\Delta t$. The radiative forcing owing to CO_2 can be calculated as $F(t) = F_0\ln[p_{CO_2}(t)/p_{CO_2}(0)]$, where $F_0 = 5.35\,\mathrm{W\,m^{-2}}$ is the radiative forcing coefficient for CO_2. We can therefore write:

$$F(t) = \lambda(t)T_a(t) + N(t) = F_0\ln[p_{CO_2}(t)/p_{CO_2}(0)]. \tag{9}$$

We assume linearity of the response in equation (9), as is commonly done, because we are only interested in an order-of-magnitude calculation, and nonlinear responses are second order. Combining equations (8) and (9), we obtain the heat content change over Δt as:

$$\hat{H}(t) = AF_0\ln[p_{CO_2}(t)/p_{CO_2}(0)]\Delta t - A\lambda(t)T_a(t)\Delta t. \tag{10}$$

Neglecting the anthropogenic carbon uptake by the land, and assuming that p_{CO_2} of the surface of the ocean is in equilibrium with the atmosphere[41] (which follows the argument that the pattern of surface ocean p_{CO_2} does not change under climate change, as outlined above), we can use the definition of the Revelle buffer factor R_{DIC}:

$$R_{DIC} = \frac{\Delta\overline{p_{CO_2}}}{\Delta\overline{DIC}}\frac{\overline{DIC}}{\overline{p_{CO_2}}} \approx \frac{\Delta I_a}{\Delta I_o}\frac{I_o}{I_a}. \tag{11}$$

Here, I_o is the pre-industrial global ocean inventory of carbon, $I_o = V\overline{DIC}$ (where V is the volume of the ocean), and I_a is the atmospheric inventory of carbon. In the formal definition of R_{DIC}, $\overline{DIC}$ is the mean surface ocean DIC concentration. However, the ratio $\overline{DIC}/\Delta\overline{DIC}$ only differs by 1% in ESM2M if we consider the mean of DIC across the upper 2,000 m instead of the surface of the ocean (and similarly in the estimate of total and anthropogenic ocean DIC from ref. [24]). The overline indicates an average over the ocean area (for p_{CO_2}) and over the volume—of the upper 2,000 m, in our case—for DIC. We can therefore write:

$$\ln\left(\frac{p_{CO_2}(t)}{p_{CO_2}(0)}\right) = \ln\left(1 + \frac{\Delta p_{CO_2}(t)}{p_{CO_2}(0)}\right) \approx \frac{\Delta p_{CO_2}(t)}{p_{CO_2}(0)} = \frac{R_{DIC}\hat{C}_{ant}(t)}{I_o(0)} \tag{12}$$

where $\hat{C}_{ant}(t) = \Delta I_o$ is total ocean anthropogenic carbon. In our approximation, $I_o(0) = I_o$, so we can re-write equation (10) as follows:

$$\hat{H}(t) = \frac{R_{DIC}AF_0}{I_o}\hat{C}_{ant}(t)\Delta t - A\lambda(t)T_a(t)\Delta t, \tag{13}$$

leading to the final equation for the linearly approximated heat–carbon coupling parameter $\tilde{\alpha}$ in a one-dimensional model:

$$\tilde{\alpha} = \frac{\hat{H}(t)}{\hat{C}_{ant}(t)} = \frac{R_{DIC}AF_0}{I_o}\Delta t - A\lambda(t)\frac{T_a(t)}{\hat{C}_{ant}(t)}\Delta t. \tag{14}$$

The left- and right-hand sides of equation (14) are shown in Extended Data Fig. 2, for the ESM2M 1%CO_2 simulation. The first term of the right-hand side of equation (14)—which depends on carbon buffering effects—captures the magnitude of α, but has too steep a slope. The second term of the right-hand side of equation (14) acts to flatten out the behaviour of the coupling parameter with time. To first order, α therefore does not depend on $\hat{H}(t)$ or $\hat{C}_{ant}(t)$ explicitly, but instead is set by F_0, R_{DIC} and I_o, which we have approximated as constants in this simple formulation. The results imply that the strength of CO_2 as a greenhouse gas, the buffer factor and the pre-industrial ocean carbon content (which is linked to the pre-industrial ocean stratification)—all of which are intrinsic quantities of the pre-industrial climate system—lead to a tight coupling between $\hat{H}$ and $\hat{C}_{ant}$, and as a result a tight coupling between H_{ad} and C_{ant}. The parameters R_{DIC} and I_o only vary up to 15% across different models, scenarios and observations, and so the spread in α across models and observations is due to the T_a term in equation (14), reflecting differences in non-CO_2 forcing agents and variations in various climate feedback processes. Over the historical period, natural variability in atmospheric warming trends probably also explains part of the large spread in α.

The error in $\tilde{\alpha}(t)$ as estimated using equation (14), compared to the diagnosed $\alpha(t)$ is due to the assumption of linearity, and that the land does not absorb any carbon. In realistic scenarios, the land is both a sink and a source of carbon, owing to differing land use. In 2009, the cumulative land sink and sources could balance, although the uncertainty on this number is large[21]. The error arising from land-use uncertainty is therefore a large component in the idealized 1%CO_2 simulation, but may have less importance in the real world. Similarly, the 1%CO_2 simulation also does not include radiative forcing from other greenhouse gases or aerosols. These effects are thought to be largely similar in magnitude but opposite in sign, and therefore to a large extent cancel out[56]. Nonetheless, equation (14) shows that, owing to intrinsic variables of the climate system, the relationship between H and C_{ant} is linear to first order, explaining why the values of α are similar across the ESM2M, MITgcm and CMIP5 models and observations.

MITgcm

We compare the results from our ESM2M simulations to ocean-only simulations using the MITgcm, in which the atmospheric forcing remains constant. We do this, first, to demonstrate that our method holds for various modelling set-up and conditions. Second, the goal of using anthropogenic carbon to estimate the fixed-circulation anthropogenic heat content is to be able to apply this method to CMIP5 models and observations. In the ESM2M simulations, the atmospheric circulation and temperatures are different in the fixed-circulation and free-circulation experiments[7]. Using an ocean-only model with fixed boundary conditions, we can show that the coupling of the ocean's heat and carbon storage is independent of ocean–atmosphere coupling.

Our global MITgcm[57] set-up uses a 1° × 1° horizontal resolution and 42 vertical levels with a realistic bathymetry. The model has a biological module[58] that resolves five tracers: DIC, ALK, PO_4, dissolved organic phosphorus (DOP) and O_2. The model is forced at the surface with NCEP reanalysis wind stress and freshwater flux[59], and the surface

Article

temperature and salinity are restored towards Levitus' monthly temperature and salinity climatology[60] to avoid model drift. We use this ocean-only model to perform free-circulation and fixed-circulation climate change experiments that resemble those performed with the ocean–atmosphere coupled GFDL ESM2M described in the text.

In testing the fixed-circulation experiments, the seasonality of the surface forcing alongside a prescribed yearly mean circulation field produces strong atmosphere–ocean flux anomalies, leading to unphysical feedback. We therefore spin up the model both for the free-circulation and fixed-circulation experiments using October conditions without a seasonal cycle. October is chosen because it produces a mean-state circulation and air–sea carbon and heat fluxes most similar to the yearly climatology of the model that is forced with the full monthly varying forcing fields. The mean overturning and barotropic streamfunctions, Ψ_{MOC} and Ψ_{BARO}, respectively, are shown in Extended Data Fig. 9.

To simulate anthropogenic warming due to CO_2 emissions, we perturb the prescribed zonally uniform climatological temperature restoring profile with a latitudinally varying temperature perturbation. The idealized perturbation curve prescribes a smooth transition from a warming of 0 °C at 90° S, to 1.5 °C at the equator, to 0.5 °C at 90° N. We introduce anthropogenic carbon by raising the value of atmospheric p_{CO_2} from 280 ppm in the pre-industrial state to 560 ppm in the first time step of the climate change experiment, after which time the carbon cycle model evolves freely (therefore adding a pulse injection of carbon). We perform this experiment with both fixed and free ocean circulation.

In the free experiment, the circulation is changing owing to the changes in surface temperature, whereas in the fixed experiment the circulation (the 3D Eulerian and bolus velocity fields) is fixed and set to its pre-industrial value. However, parameterizations such as convective and eddy mixing are allowed to act freely for the both the free-circulation and fixed-circulation experiments, as in ESM2M. To remove the effects of the drift in the fixed-circulation warming experiment, we run a tandem fixed-circulation pre-industrial control simulation. All anomalies are calculated as the difference between the perturbation experiment and the tandem control simulation. After 50 yr (100 yr), there is a 3% (4%) difference in total ocean anthropogenic carbon uptake between the fixed-circulation and free-circulation experiments, and a 4% (6%) difference in total heat storage, which agrees well with previous coupled climate simulations[7]. The total ocean heat and carbon uptake are therefore similar between the free-circulation and fixed-circulation experiments, although their spatial distributions are different.

The perturbed overturning and barotropic streamfunctions, Ψ_{MOC} and Ψ_{BARO}, respectively, are shown in Extended Data Fig. 9. The experiments have been designed to optimally and rigorously test the presented method. Therefore, our scenarios are idealized, inducing large warming-induced circulation changes, instead of inducing realistic climate change scenarios from historical forcing or projections. However, our model simulations show very similar quantitative and qualitative results to coupled climate models under climate change scenarios as well as observational patterns of ocean warming and anthropogenic carbon storage[7,24,61–63].

The results for fixed-circulation and free-circulation 0–2,000 m column-integrated anthropogenic heat and carbon storage, as well as for the carbon and heat redistribution, are shown in Extended Data Fig. 10. Extended Data Fig. 10 also shows the fixed circulation and redistributed heat content, as calculated using only free-circulation quantities and equations (1) and (2). Similarly to fully coupled climate model experiments[7], discrepancies in the patterns of anthropogenic heat content between the free-circulation and fixed-circulation simulations are apparent, whereas patterns of anthropogenic carbon storage remain largely unaffected by changes in ocean currents that arise from warming. After 70 yr, the anthropogenic heat storage in the fixed experiment, H_{ad}, has increased in all regions, whereas in

the free experiment, the ocean heat storage H has decreased in the North Atlantic and more heat is stored in the low latitudes in the South Atlantic. The pattern of anthropogenic heat storage in the Atlantic is due to the redistribution of heat by the modified circulation as the weakening of the Atlantic meridional overturning circulation can lead to a reduction of heat transport from the South Atlantic to the North Atlantic[11,13,61,62]. The redistribution of anthropogenic carbon however, is much smaller.

The fixed heat that is calculated using equations (1) and (3) (Extended Data Fig. 10) agrees very well with the explicitly simulated fixed heat. The corresponding redistributed heat patterns are also similar to those calculated using the fixed-circulation experiment, demonstrating the usefulness of our method for models with different structure and forcing.

Significance testing

To test the statistical significance of the redistributed heat in the CMIP5 ensemble, we test at the 66% confidence level. The redistributed heat is not significant where the mean signal is less than $\sigma/\sqrt{N}$, where σ is the standard deviation of the signal and N is the number of CMIP5 models, $N = 11$. The mean state has a zero mean and zero standard deviation of redistributed heat.

To test the significance of the redistributed heat in the observations, we test at the 66% confidence level by calculating whether the signal is larger than the 1σ confidence interval. The 1σ confidence interval is determined by quadratically combining the 1σ uncertainty in the observational estimates of heat and carbon storage.

CMIP5

The 11 CMIP5 models used in this study are the following: CMCC-CESM, CNRM, IPSL-CM5A LR, IPSL-CM5A MR, IPSL-CM5B LR, HadGEM2-ES, HadGEM2-CC, MPI ESM MR, NorESM, GFDL ESM2M and GFDL ESM2G. All of these models are Earth system models with fully coupled carbon cycles. Heat and carbon anomalies are calculated with respect to a tandem 1850 pre-industrial control simulation.

Data availability

The code of the GFDL ESM2M model is available from https://github.com/mom-ocean and the results from the free-circulation and fixed-circulation 1%CO_2 simulations are available from https://doi.org/10.1594/PANGAEA.914424. CMIP5 model data are available from the Earth System Grid Federation data portal at https://esgf-node.llnl.gov/projects/cmip5/. The historical ocean temperature reanalysis[23] from is available at http://159.226.119.60/cheng/. The estimate of historical ocean anthropogenic carbon[24] is available at https://tdevries.eri.ucsb.edu/models-and-data-products/. The observed ocean heat uptake[10] is available at https://laurezanna.github.io/publication/zanna-et-al-2017b/. The MITgcm code is available at http://mitgcm.org/. The GLODAPv2 synthesis product is available at https://www.nodc.noaa.gov/ocads/oceans/GLODAPv2/. The topographical data used in Figs. 1, 3, 4 and Extended Data Figs. 1, 5, 8–10 are available in MATLAB and provided by NOAA[64]. The CMIP5 and observational estimates of total, added and redistributed heat are available at https://laurezanna.github.io/publication/bronselaer-zanna-2020/.

39. Dunne, J. P. et al. GFDL's ESM2 global coupled climate–carbon Earth system models. Part I: Physical formulation and baseline simulation characteristics. *J. Clim.* **25**, 6646–6665 (2012).
40. Dunne, J. P. et al. GFDL's ESM2 global coupled climate–carbon Earth system models. Part II: Carbon system formulation and baseline simulation characteristics. *J. Clim.* **26**, 2247–2267 (2013).
41. Fay, A. R. & McKinley, G. A. Global trends in surface ocean p_{CO_2} from in situ data. *Glob. Biogeochem. Cycles* **27**, 541–557 (2013).
42. Tjiputra, J. F. et al. Long-term surface p_{CO_2} trends from observations and models. *Tellus B* **66**, 23083 (2014).
43. Fine, R. A., Peacock, S., Maltrud, M. E. & Bryan, F. O. A new look at ocean ventilation time scales and their uncertainties. *J. Geophys. Res. Oceans* **122**, 3771–3798 (2017).

44. Jones, D. C., Ito, T., Takano, Y. & Hsu, W.-C. Spatial and seasonal variability of the air–sea equilibration timescale of carbon dioxide. *Glob. Biogeochem. Cycles* **28**, 1163–1178 (2014).
45. Lovenduski, N. S., Gruber, N., Doney, S. C. & Lima, I. D. Enhanced CO_2 outgassing in the Southern Ocean from a positive phase of the Southern Annular Mode. *Glob. Biogeochem. Cycles* **21**, GB2026 (2007).
46. Sarmiento, J. & Gruber, N. *Ocean Biogeochemical Dynamics* (Princeton Univ. Press, 2006).
47. Takahashi, T., Olafsson, J., Goddard, J., Chipman, D. & Sutherland, S. Seasonal variation of CO_2 and nutrients in the high-latitude surface oceans: a comparative study. *Glob. Biogeochem. Cycles* **7**, 843–878 (1993).
48. Williams, R. G. et al. Nutrient streams in the north Atlantic: advective pathways of inorganic and dissolved organic nutrients. *Glob. Biogeochem. Cycles* **25**, GB4008 (2011).
49. Fine, R. A. Observations of CFCs and SF6 as ocean tracers. *Annu. Rev. Mar. Sci.* **3**, 173–195 (2011).
50. Steinacher, M. et al. Projected 21st century decrease in marine productivity: a multi-model analysis. *Biogeosciences* **7**, 979–1005 (2010).
51. Schwinger, J. et al. Nonlinearity of ocean carbon cycle feedbacks in CMIP5 Earth system models. *J. Clim.* **27**, 3869–3888 (2014).
52. Fu, W., Randerson, J. T. & Moore, J. K. Climate change impacts on net primary production (NPP) and export production (EP) regulated by increasing stratification and phytoplankton community structure in the CMIP5 models. *Biogeosciences* **13**, 5151–5170 (2016).
53. Arora, V. K. et al. Carbon–concentration and carbon–climate feedbacks in CMIP5 Earth system models. *J. Clim.* **26**, 5289–5314 (2013).
54. Randerson, J. T. et al. Multi-century changes in ocean and land contributions to climate-carbon feedbacks. *Glob. Biogeochem. Cycles* **29**, 744–759 (2015).
55. Myhre, G., Highwood, E., Shine, K. & Stordal, F. New estimates of radiative forcing due to well mixed greenhouse gases. *Geophys. Res. Lett.* **25**, 2715–2718 (1998).
56. Solomon, S. et al. (eds) *Climate Change 2007: The Physical Science Basis. Working Group I Contribution to the Fourth Assessment Report of the Intergovernmental Panel on Climate Change* (Cambridge Univ. Press, 2007).
57. Marshall, J., Adcroft, A., Hill, C., Perelman, L. & Heisey, C. A finite-volume, incompressible Navier–Stokes model for studies of the ocean on parallel computers. *J. Geophys. Res. Oceans* **102**, 5753–5766 (1997).
58. Dutkiewicz, S., Follows, M. & Parekh, P. Interactions of the iron and phosphorus cycles: a three-dimensional model study. *Glob. Biogeochem. Cycles* **19**, GB1021 (2008).
59. Kalnay, E. et al. The NCEP/NCAR 40-year reanalysis project. *Bull. Am. Meteorol. Soc.* **77**, 437–471 (1996).
60. Levitus, S. E. *Climatological Atlas of the World Ocean* NOAA Professional Paper 13 (US Department of Commerce, NOAA, 1982).
61. Stouffer, R. et al. Investigating the causes of the response of the thermohaline circulation to past and future climate changes. *J. Clim.* **19**, 1365–1387 (2006).
62. Rahmstorf, S. et al. Exceptional twentieth-century slowdown in Atlantic Ocean overturning circulation. *Nat. Clim. Chang.* **5**, 475–480 (2015); correction **5**, 956 (2015).
63. Sgubin, G., Swingedouw, D., Drijfhout, S., Mary, Y. & Bennabi, A. Abrupt cooling over the North Atlantic in modern climate models. *Nat. Commun.* **8**, 14375 (2017).
64. National Geophysical Data Center. *ETOPO5: Data Announcement 88-MGG-02, Digital Relief of the Surface of the Earth* (NOAA, 1988); https://doi.org/10.7289/V5C8276M
65. Olsen, A. et al. The Global Ocean Data Analysis Project version 2 (GLODAPv2) – an internally consistent data product for the world ocean. *Earth Syst. Sci. Data* **8**, 297–323 (2016).
66. Key, R. M.et al. *Global Ocean Data Analysis Project, Version 2 (GLODAPv2)* Report no. ORNL/CDIAC-162, ND-P093 (Carbon Dioxide Information Analysis Center, Oak Ridge National Laboratory, US Department of Energy, 2015).
67. Lauvset, S. K. et al. A new global interior ocean mapped climatology: the 1° × 1° GLODAP version 2. *Earth Syst. Sci. Data* **8**, 325–340 (2016).
68. van Heuven, S., Pierrot, D., Rae, J. W. B., Lewis, E. & Wallace, D. W. R. *MATLAB Program Developed for CO2 System Calculations* https://cdiac.ess-dive.lbl.gov/ftp/co2sys/ CO2SYS_calc_MATLAB_v1.1/ (Carbon Dioxide Information Analysis Center, US Department of Energy, 2011).
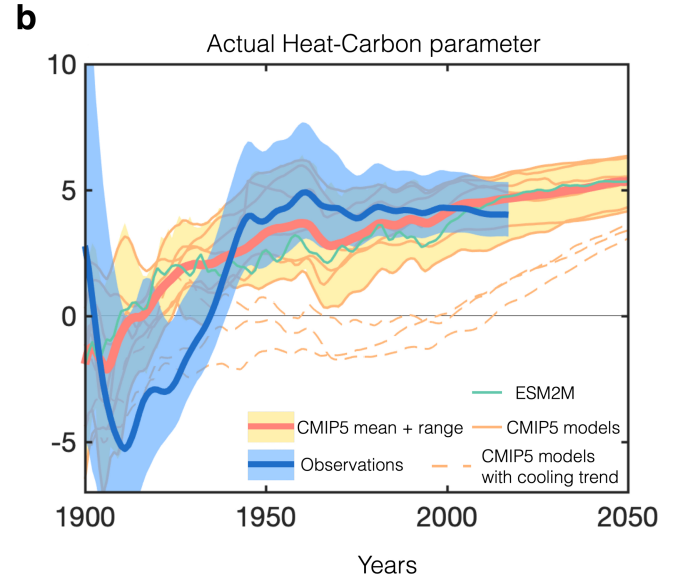
Extended Data Fig. 1 | Physical changes in ESM2M experiments. a, **b**, Using the free-circulation model, the fixed-layer depth of the pre-industrial control mean (**a**) and the change in mixed-layer depth (relative to the control) (**b**), for years 61–80 of the 1%CO$_2$ free circulation. **c**, Years 61–80 of the 1%CO$_2$ fixed-circulation simulation. In the fixed-circulation experiment, north of 30° N in the North Atlantic Ocean, there is an average reduction in mixed-layer depth of 15%, where mixed layer depths were deeper than 200 m in the control mean. **d**–**f**, As in **a**–**c**, but for the meridional overturning streamfunction, where 1 Sv = 10^6 m^3 s^{-1}. **g**–**i**, As in **a**–**c**, but for the barotropic streamfunction.
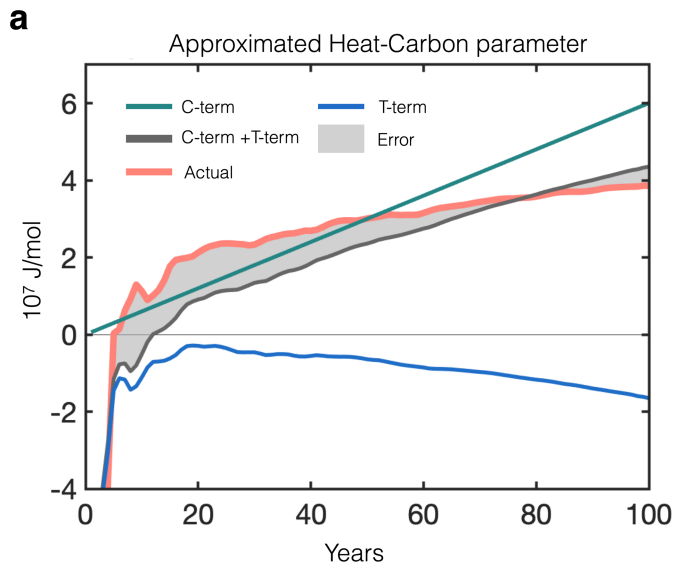
Extended Data Fig. 2 | The heat–carbon coupling parameter, α.
a, α, obtained in ESM2M using $\alpha(t) = \hat{H}(t)/\hat{C}_{ant}(t)$ (pink), and as estimated using equation (14) for $\tilde{\alpha}$ (grey line). The green line shows the magnitude of the first term of the right-hand side of equation (14), and the blue line shows the second term of the right-hand side of equation (14), which is related to the temperature-feedback term. The grey shading shows the error in the estimate that is due to the assumption of linearity and to various other processes and feedback mechanisms ignored, such as land carbon uptake. The negative values of α and $\tilde{\alpha}$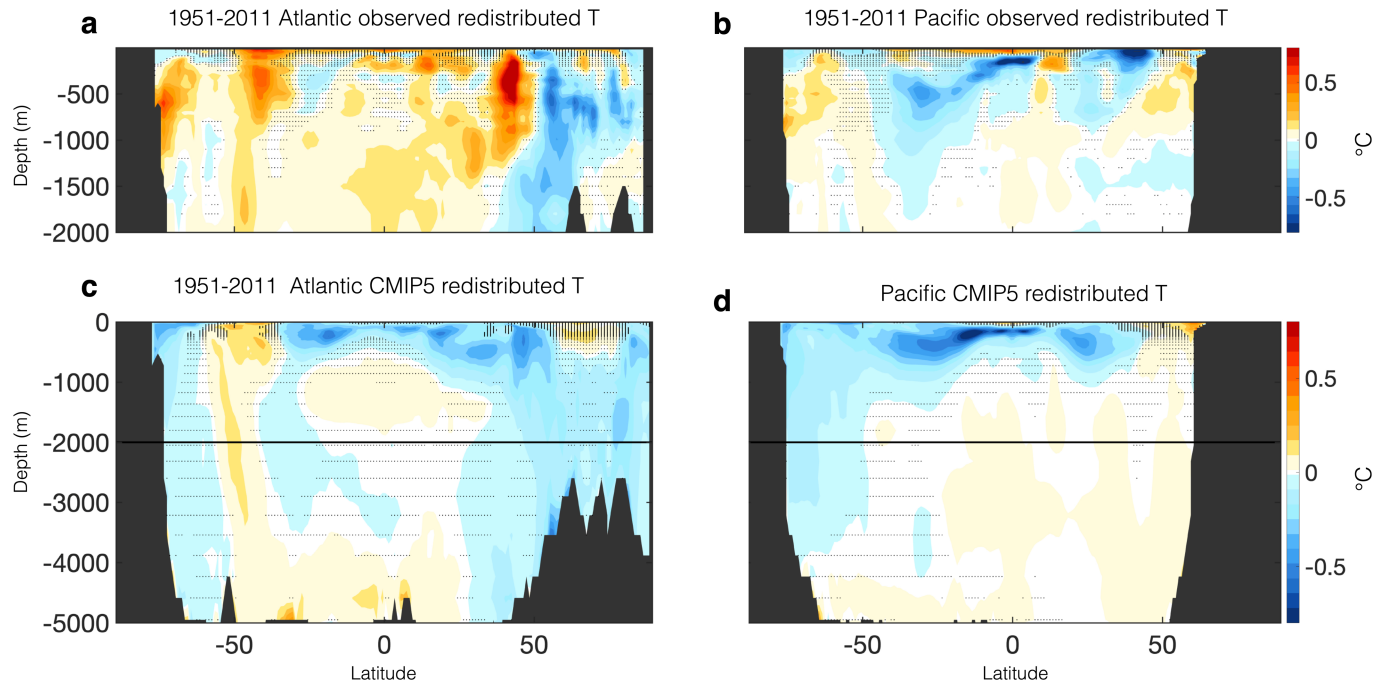 at the start of the experiment are due to natural variability when the external forcing is small (giving a low signal-to-noise ratio).
b, $\alpha(t) = \hat{H}(t)/\hat{C}_{ant}(t)$, relative to the years 1870–1890 in CMIP5 historical/RCP8.5 simulations, with the mean given by the thick pink line and the range given by the pale yellow area. Thin lines show individual models (ESM2M is shown in green for reference) and dashed lines show the models that simulate ocean heat loss in the mid-twentieth century that are excluded from the mean and range. The blue solid line shows the observations (using ref.[10] for heat) and its blue shading shows the 66% confidence interval from observations.
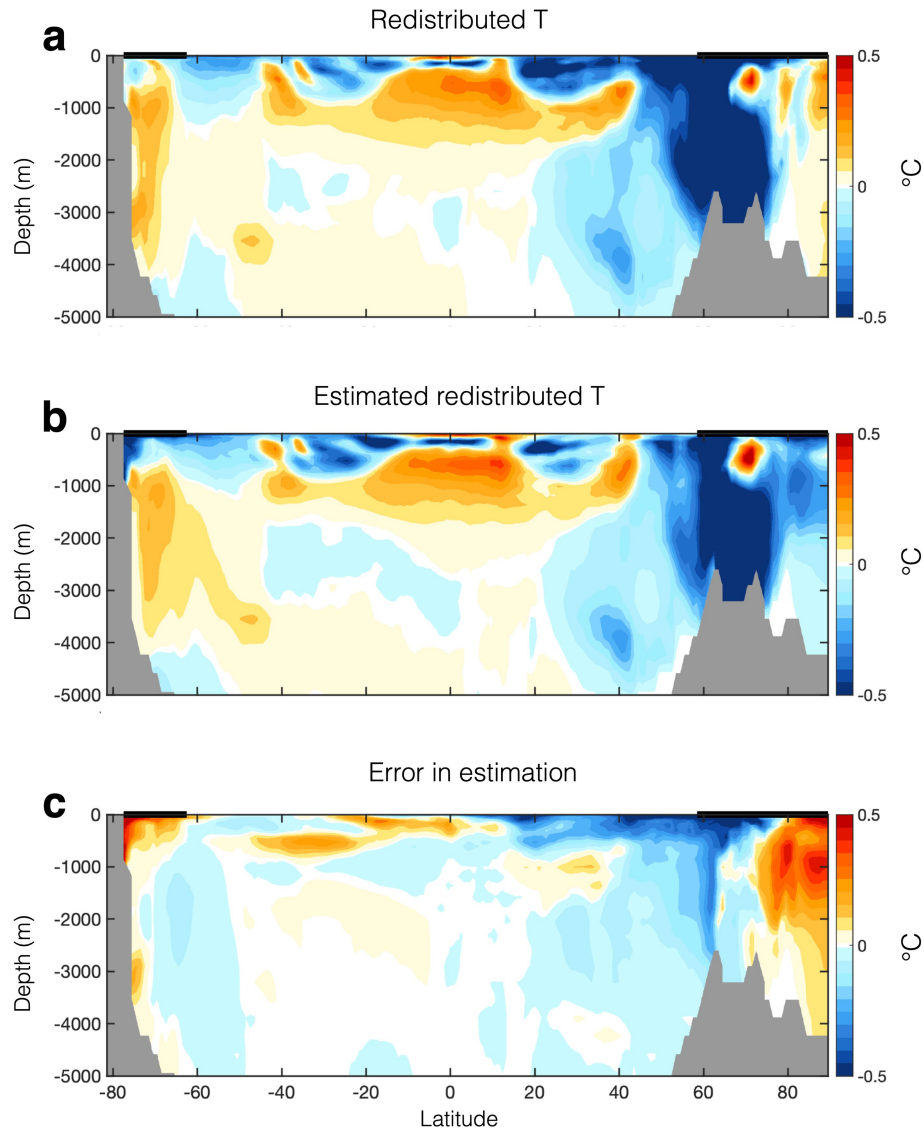
Extended Data Fig. 3 | ESM2M zonal-mean ocean redistributed warming.
a, **b**, The year 61–80 zonal-mean ocean redistributed heat, here expressed as
the zonal-mean temperature change, and calculated using the diagnosed fields
from the ESM2M fixed-circulation experiment (**a**), and using the expression
$H_{ad}(y, z, t) = \alpha(t)C_{ant}(y, z, t)$ (**b**). The parameters (y, z, t) indicate the zonal-mean

quantities instead of vertical integrals, and $\alpha(t)$ is calculated globally as before,
except here divided by volume, density and specific heat capacity so that
values are given in terms of temperature instead of heat capacity. **c**, The
difference between **a** and **b**; the black lines on the $z = 0$ axis show the mean
sea-ice extent.

a 1951-2011 Atlantic observed redistributed T

b 1951-2011 Pacific observed redistributed T

c 1951-2011 Atlantic CMIP5 redistributed T

d Pacific CMIP5 redistributed T

Extended Data Fig. 4 | 1951–2011 zonal-mean ocean redistributed warming.
Ocean redistributed heat $H_{ad}(y, z, t) = \alpha(t)C_{ant}(y, z, t)$ in terms of temperature
instead of than heat. Changes are shown as the linear trends over the indicated
periods multiplied by the length of the period. **a**, **b**, The results from
observational estimates for the Atlantic basin (**a**) and the Pacific basin (**b**).
c, **d**, Changes in the CMIP5 historical RCP8.5 ensemble. The black horizontal
line indicates the 2,000 m depth level above which we show the observations.
The hatching indicates where the changes are not significant at the 66%
uncertainty level. For the observations, the uncertainty is from the estimates
of H and C_{ant}, whereas for the CMIP5 models the uncertainty is from the mean of
the ensemble due to inter-model spread.

a

H_r **CMIP5** 1951-2011 - **top 3 models**

b

H_r **CMIP5** 2011-2050 - **top 3 models**
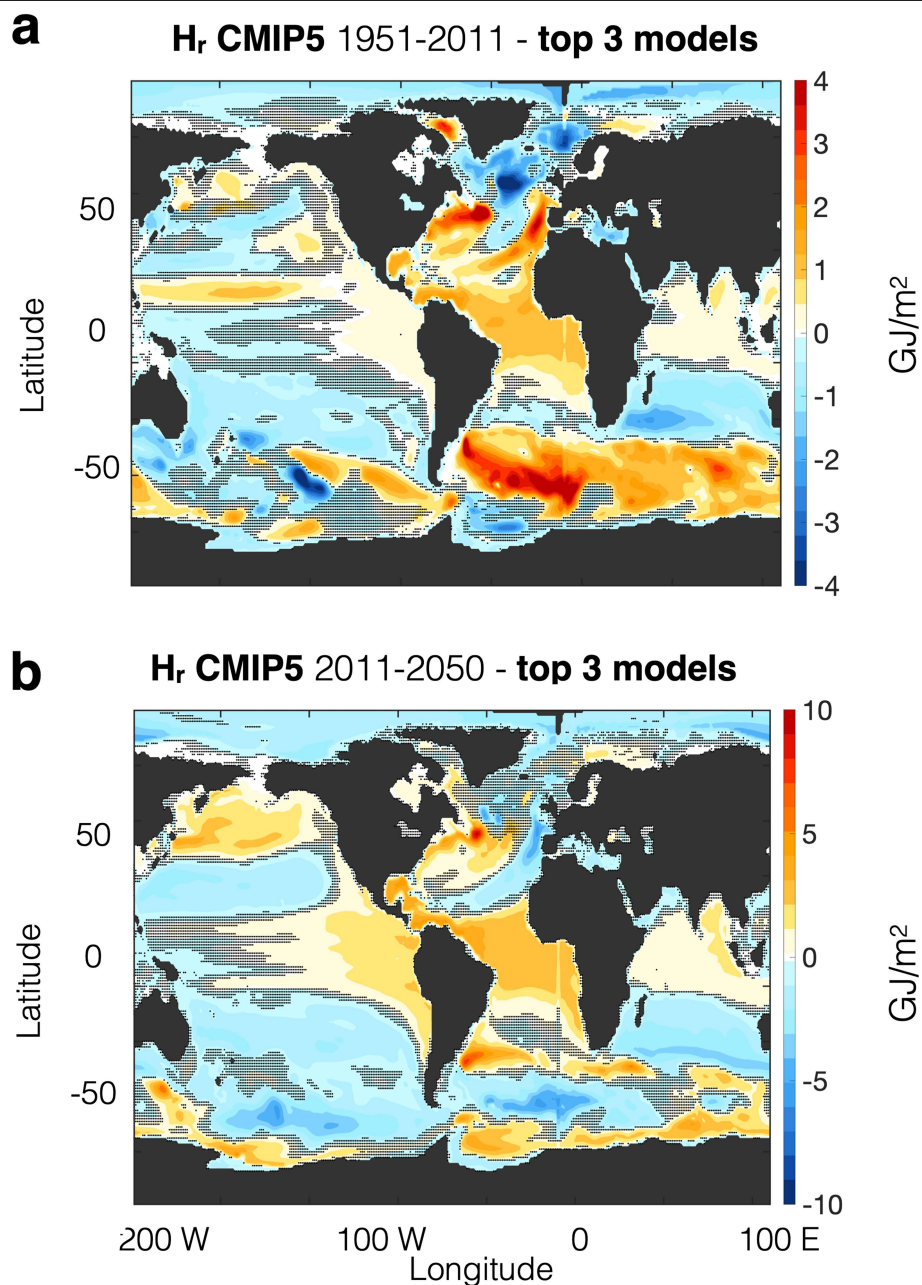
Extended Data Fig. 5 | CMIP5 ocean redistributed heat. a, Average 1951–2011 H_r for the three CMIP5 models (CNRM-CM5, GFDL ESM2M and GFDL ES2MG) with a value of H_r that best match the observational reconstruction. **b**, Average 2011–2060 H_r for the same models as in **a**. The hatching indicates where the changes are not significant at the 66% uncertainty level; the uncertainty is from the mean of the ensemble due to inter-model spread.
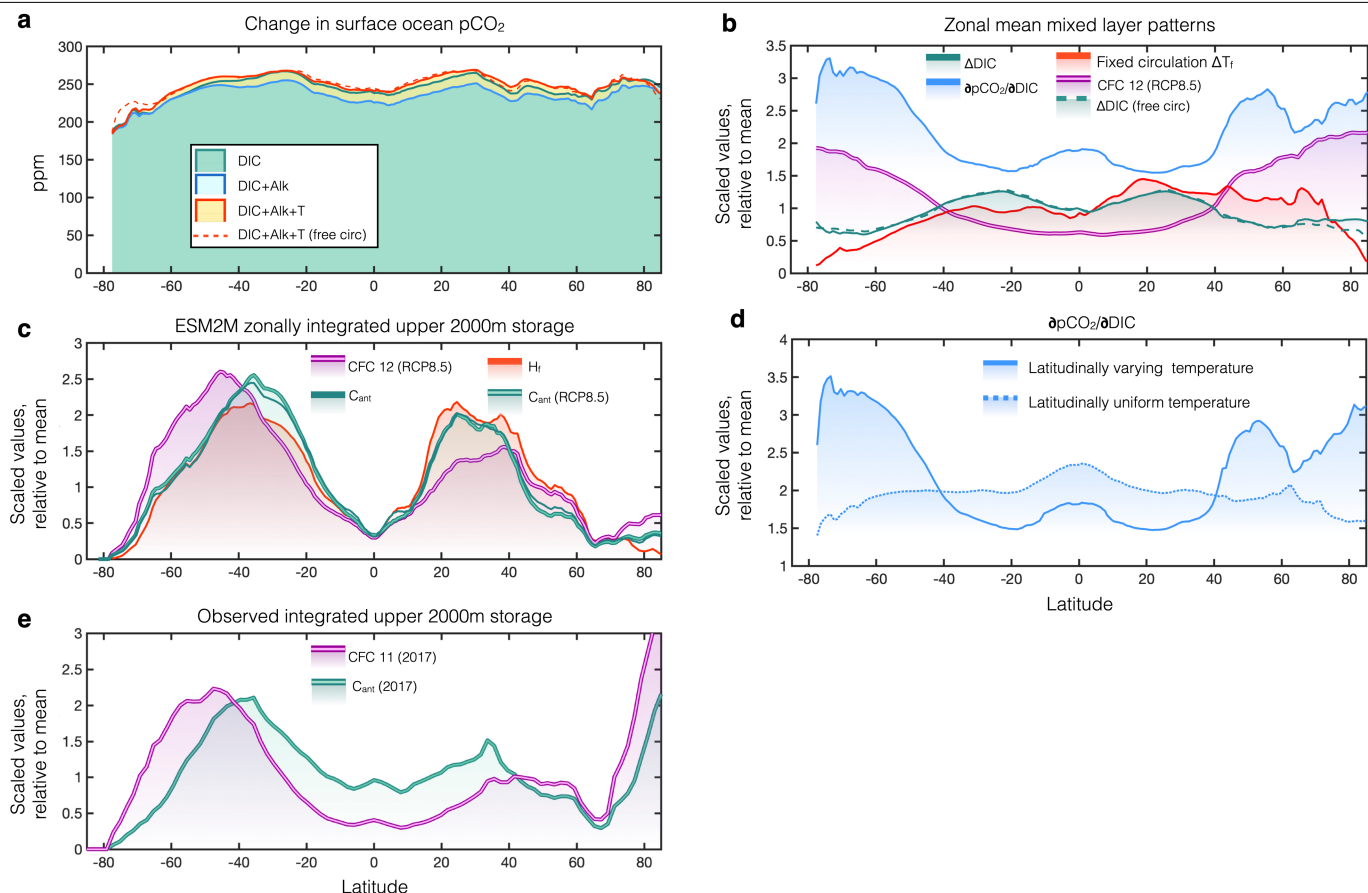
**Extended Data Fig. 6 | Latitudinal profiles of ocean carbon and CFCs.**
a, ESM2M zonal-mean contribution of DIC (green), DIC+ALK (blue) and
DIC+ALK+T (red) towards the change in ocean surface p_{CO_2}. Changes in p_{CO_2}
(Δp_{CO_2}), are roughly equal to $(\partial p_{CO_2}/\partial DIC)\Delta DIC$. **b**, ESM2M zonal-mean mixed
layer change, relative to the pre-industrial control, in ΔDIC (green),
fixed-circulation added temperature ΔT_{ad} (red), and $\Delta CFC12$ (purple). The blue
line shows the sensitivity term $\partial p_{CO_2}/\partial DIC$. **c**, ESM2M zonally integrated C_{ant}
(green), CFC 12 (purple) and H_{ad} (red) storage in the upper 2,000 m relative to

the pre-industrial control. Solid single lines show year 70 from the
fixed-circulation 1%CO_2 and double lines show year 2060 of the ESM2M RCP8.5
simulation. **d**, ESM2M $\partial p_{CO_2}/\partial DIC$ with a latitudinally varying temperature
(solid) and a latitudinally constant temperature (dotted). **e**, Observed zonally
integrated C_{ant} (green) and CFC 11 (purple) storage in the upper 2,000 m in
year 2017, from ref. [24]. The quantities in **b**–**d** have been scaled by the global
mean value for each tracer, and the blue line in **b** has been offset upwards by a
scaled value of 1 for clarity.
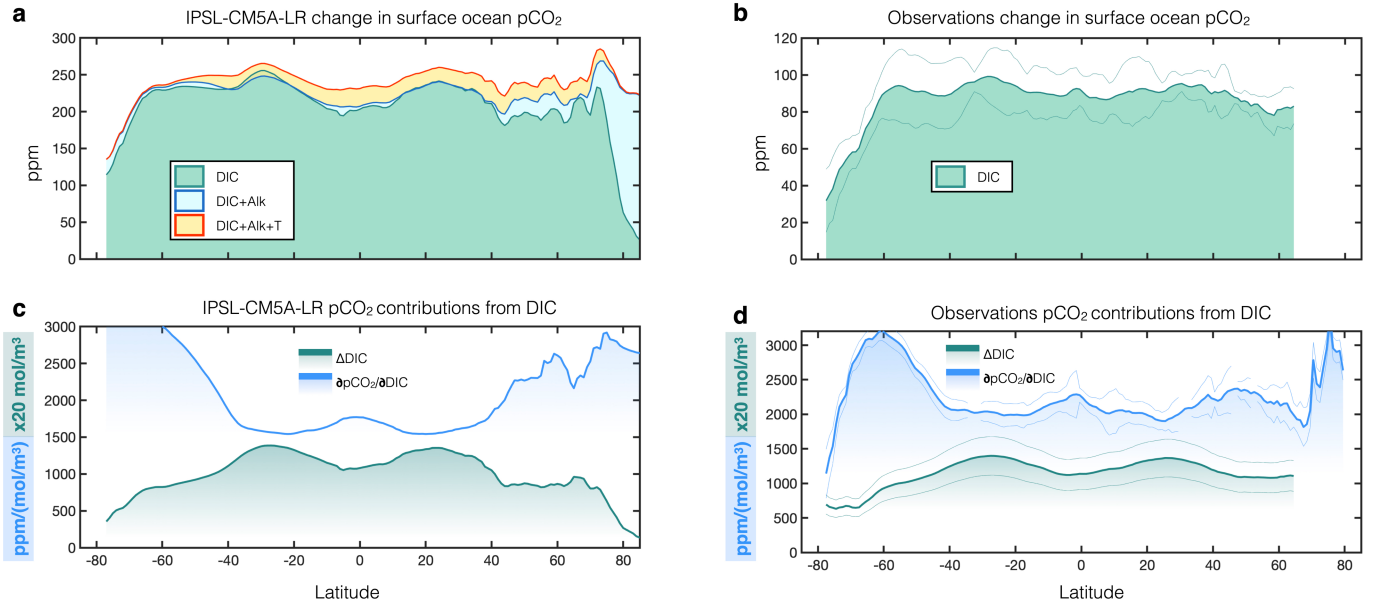
Extended Data Fig. 7 | Latitudinal p_{CO_2} changes. a, **b**, Zonal-mean contribution of DIC (green), DIC + ALK (blue) and DIC + ALK + T (total; red), towards the change in ocean surface p_{CO_2} at year 70 of the 1%CO_2 simulation with IPSL-CM5A-LR, relative to the pre-industrial control (**a**), and at year 2011 best-estimate from observations, relative to year 1765, using GLODAPv2[65–67] for mean-state fields and ΔDIC (C_{ant}) from ref. [24]. **c**, **d**, Zonal-mean contribution of ΔDIC (green) and $\partial p_{CO_2}/\partial$DIC (blue) towards ocean surface p_{CO_2} changes at year 70 of the 1%CO_2 simulation with IPSL-CM5A-LR (**c**), and year 2011 from observations (using GLODAPv2 for mean states fields[37] and ΔDIC from ref. [24]; **d**). The thin lines in **b** and **d** show the 66% confidence interval. p_{CO_2} values from observations are calculated using CO2SYS[68]. The correlation coefficients between ΔDIC and $\partial p_{CO_2}/\partial$DIC are −0.88 and −0.82 for IPSL-CM5A-LR and observations, respectively.
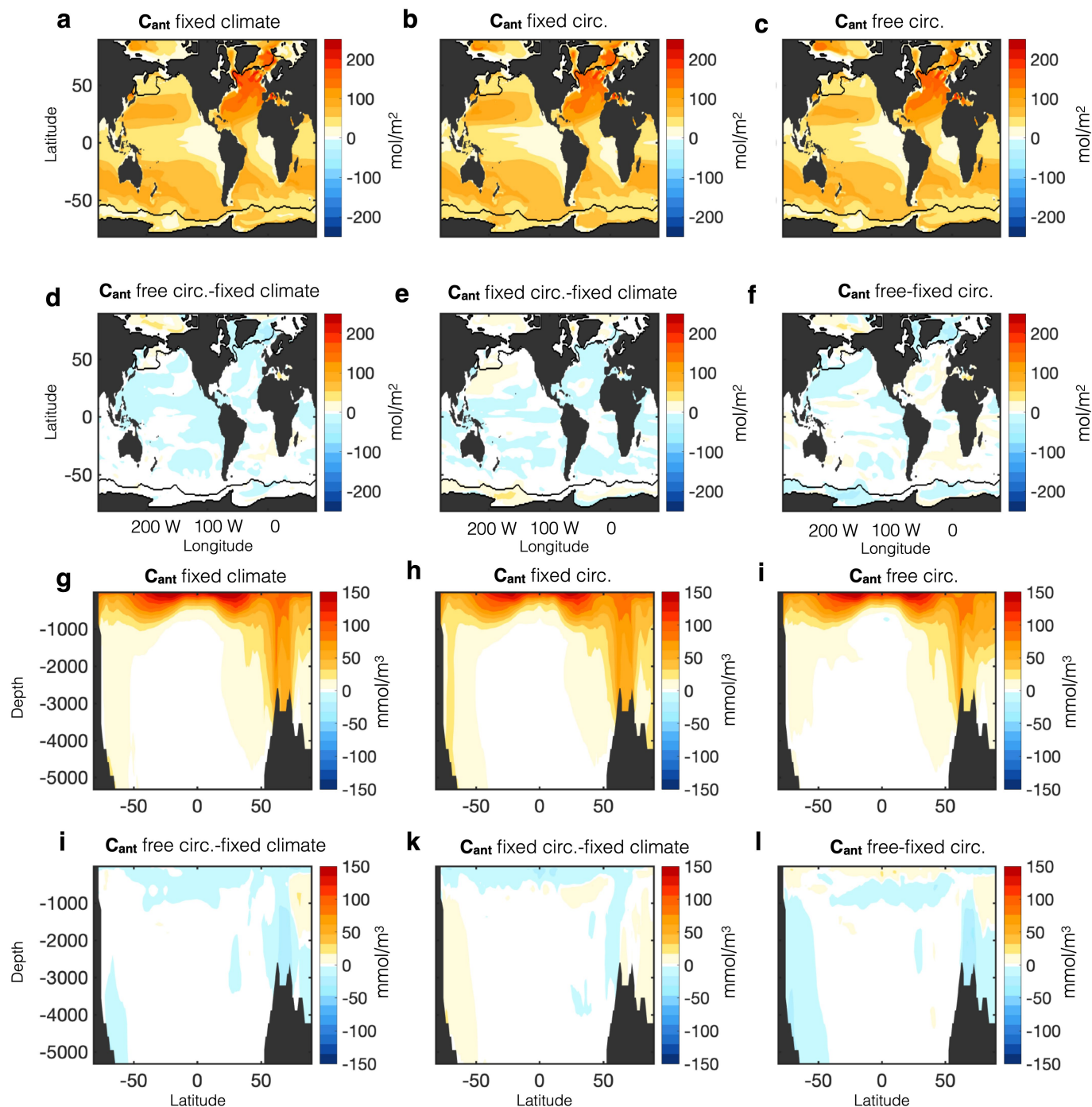
Extended Data Fig. 8 | Fixed-climate C_{ant}. a–c, Year 61–80 mean upper 2,000 m C_{ant} in the fixed-climate (**a**), fixed-circulation (**b**) and free-circulation (**c**) 1%CO_2 ESM2M simulations. In the fixed-climate simulation, atmospheric CO_2 is treated as a non-radiative gas[29]. The correlation coefficients of the fixed-circulation and fixed-climate C_{ant}, with free-circulation C_{ant} as shown, are 0.98 and 0.98, respectively. **d**, The difference between the free-circulation and fixed-climate experiments. **e**, The difference between the fixed-circulation and fixed-climate experiment. **f**, The difference between the free-circulation and fixed-circulation experiments. **g–l**, As in **a–f**, but for zonal-mean C_{ant}.

a Mean ψ$_{MOC}$

b Mean ψ$_{BARO}$

c ψ$_{MOC}$ change

d ψ$_{BARO}$ change
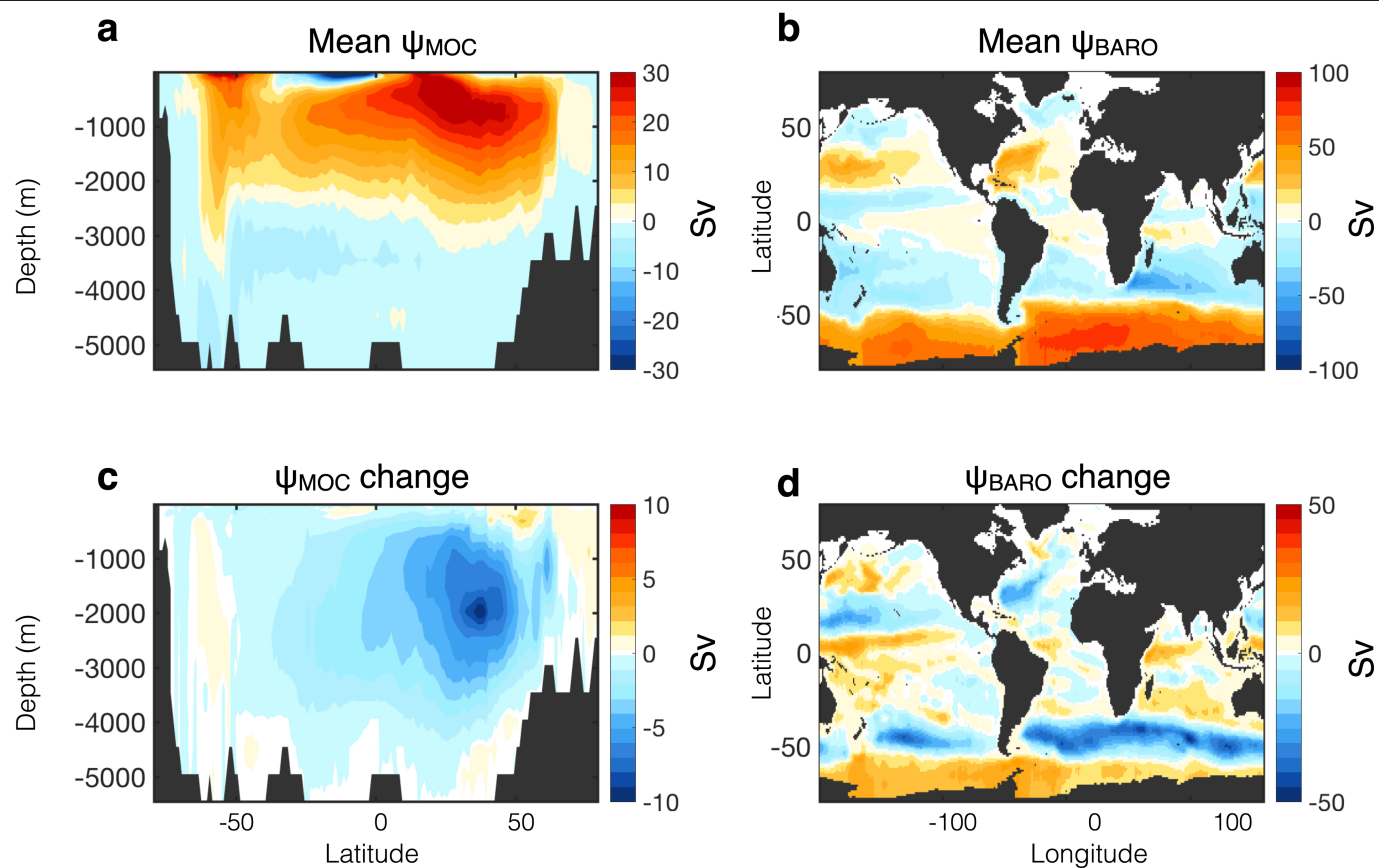
Extended Data Fig. 9 | MITgcm ocean circulation. a, b, The mean-state (**a**) and overturning (**b**) barotropic streamfunctions in the MITgcm control simulation, where $1\,\mathrm{Sv} = 10^6\,\mathrm{m}^3\,\mathrm{s}^{-1}$. **c, d**, The perturbed (**c**) and overturning (**d**) barotropic streamfunctions in the MITgcm climate change simulation after 70 yr of warming (taken as the mean of years 61–80).